Federal University of Espírito Santo

Technological Center

Postgraduate Program in Electrical Engineering

GIANCARLO PEDRONI DEL PIERO

INTERACTION OF AN EMOTION RESPONSIVE ROBOT AND CHILDREN WITH AUTISM SPECTRUM DISORDER USING CONTROLLER BASED ON PROXEMICS

Brazil

2021

GIANCARLO PEDRONI DEL PIERO

INTERACTION OF AN EMOTION RESPONSIVE ROBOT AND CHILDREN WITH AUTISM SPECTRUM DISORDER USING CONTROLLER BASED ON PROXEMICS

Dissertation submitted for the Postgraduate Program in Electrical Engineering, Federal University of Espírito Santo as a preliminary requirement to obtain the Master's degree in Electrical Engineering.

Supervisor: Professor Phd Teodiano Freire Bastos Filho

Brazil

2021

Ficha catalográfica disponibilizada pelo Sistema Integrado de
Bibliotecas - SIBI/UFES e elaborada pelo autor

PIERO, GIANCARLO PEDRONI DEL, 1979-

P615i Interaction of an emotion responsive robot and children with autism spectrum disorder using controller based on proxemics / GIANCARLO PEDRONI DEL PIERO. - 2021.

97 f. : il.

Orientador: Teodiano Freire Bastos Filho.

Dissertação (Mestrado em Engenharia Elétrica) - Universidade Federal do Espírito Santo, Centro Tecnológico.

1. Autism Spectrum Disorder. 2. Mobile Social Robot. 3. Emotions. 4. Control. 5. ROS. I. Bastos Filho, Teodiano Freire. II. Universidade Federal do Espírito Santo. Centro Tecnológico. III. Título.

CDU: 621.3

GIANCARLO PEDRONI DEL PIERO

INTERACTION OF AN EMOTION RESPONSIVE ROBOT AND CHILDREN WITH AUTISM SPECTRUM DISORDER USING CONTROLLER BASED ON PROXEMICS

Dissertation submitted for the Postgraduate Program in Electrical Engineering, Federal University of Espírito Santo as a preliminary requirement to obtain the Master's degree in Electrical Engineering.

Approved on September 22, 2021.

Examined by:

Professor Phd Teodiano Freire Bastos-Filho
Federal University of Espírito Santo
Supervisor

Phd Eliete Maria de Oliveira Caldeira
Federal University of Espírito Santo
Jury

Phd Daniel Cruz Cavalieri
Federal Institute of Espírito Santo
Jury

A Deus dedico todo o meu ser.

ACKNOWLEDGEMENTS

À minha mãe, Ana Maria, e ao meu pai, Geraldo[1], por terem me concebido e me criado.

À minha amada esposa Luciana. Companheirismo, paciência, carinho, amizade, incentivo, são muitos os adjetivos que te qualificam.

Aos meus filhos Luigi e Rafael, que entenderam (quase sempre) o motivo da minha dedicação ao mestrado. Foram muitos os momentos que precisei parar a pesquisa ou a escrita deste texto para brincar com vocês e isso foi um estímulo (como uma recarga de energia).

Aos professores e às professoras que contribuíram na minha carreira acadêmica, desde a creche até o momento atual.

Em especial, ao professor Dr. Teodiano, pelo incentivo e pela disposição em partilhar deste projeto tão significante, e à professora Dra. Eliete, pela ajuda, pela paciência, pelo estímulo a continuar, pelas revisões dos artigos publicados e pela colaboração contínua.

[1] em memória, † 08 de junho de 2008

"Whatsoever thy hand findeth to do, do it with thy might; for there is no work, nor device, nor knowledge, nor wisdom, in the grave, whither thou goest."

(The Bible, Ecclesiastes, 9, 10)

ABSTRACT

Children with Autism Spectrum Disorder (ASD) who are diagnosed early and therefore receive appropriate treatment can improve their development. One way to encourage them is using social robots. This Master's Dissertation presents an improvement for the robot created by the Assistive Technology and Robotics Group at UFES using proxemics. A new control law using the *Workspace* concept and an internal representation with an external visualization of the robot's emotional state are also presented. The Robot Operating System (ROS) is incorporated into the design to facilitate modifications and adaptations. The results show that proxemics influences the robot's controllability, as proposed through the *State Machine*, and respects the child's wishes, and that the robot is able to simulate emotions during its movement and according to its interaction with the child.

Keywords: Autism Spectrum Disorder. Mobile Social Robot. Emotions. Control. ROS.

RESUMO

Crianças com Transtorno do Espectro Autista (TEA) que são diagnosticadas precocemente e que por isso recebem um tratamento apropriado podem aperfeiçoar os seus desenvolvimentos. Uma forma de estimulá-las é utilizando robôs sociais. Esta Dissertação de Mestrado apresenta uma melhoria para o robô criado pelo Núcleo de Tecnologia Assistiva da UFES usando proxêmica. Uma nova lei de controle utilizando o conceito de *Workspace* e uma representação interna com uma visualização externa do estado emocional do robô também são apresentadas. O Sistema Operacional para Robôs (ROS) é incorporado ao projeto para facilitar as modificações e as adaptações. Os resultados mostram que a proxêmica influencia na controlabilidade do robô, conforme foi proposto através da *Máquina de Estados*, e respeita os desejos da criança, e que o robô consegue simular emoções durante seu deslocamento e de acordo com sua interação com a criança.

Palavras-chave: Transtorno do Espectro Autista. Robótica Social Móvel. Emoções. Controle. ROS.

LIST OF FIGURES

LIST OF TABLES

LIST OF SYMBOLS

X^R	Robot's Axis X
Y^R	Robot's Axis Y
X^W	World's Axis X
Y^W	World's Axis Y

CONTENTS

1 INTRODUCTION

> Apply thine heart unto instruction, and thine ears to the words of knowledge.
>
> Proverbs, 23, 12

Robots are used since 1960's, when General Motors introduced the *Ultimate*, an assistant in automobile production's assembly line. Since then, research on the use of robots has grown every year, as can be visualized on Figure 1 (COCCIA, 2018).

The use of robots as a healthcare assistant grew in the same proportion (KUJAT, 2010; STONE et al., 2016). Robots can be used to deliver specimens, medications or supplies; to help people eating; to facilitate a communication as a two-way video calling; to aid therapy of developmentally disabled children; or to help paralyzed patients walk or balance (COELHO, 2014). They can be also used to provide assistance or comfort for patients or visitors; to improve patient recovery time; in disease detection and treatment; or just as a bedside companion (MATTHEWS, 2019). Yates, Vaessen and Roupret (2011) and Bogue (2011) presented how robots have been used in healthcare, specially in surgery in urology and prosthetic.

There are various studies on how to use robots in developmental therapies with children with disabilities, specially in children with Autism Spectrum Disorder (ASD) (ZHANG et al., 2019; ISMAIL et al., 2019; CABIBIHAN et al., 2013). A specific use of social robot is to help autism community on diagnosis (SCASSELLATI, 2007; DUQUE, 2019).

After diagnosis, continuous treatment through multidisciplinary therapies is very important (MICHAUD; CLAVET, 2001; SCASSELLATI; ADMONI; MATARIĆ, 2012). Among the various strategies adopted for interaction with children with ASD, there is one that uses robots. The adoption of the interaction between robots and children with ASD aims to stimulate the creation of bonds between these children and their parents, caregivers and therapists (BINOTTE, 2018).

Robotics has been increasingly used for therapeutic purposes in order to allow individuals to develop their cognitive, social or behavioral skills (TAPUS; TAPUS; MATARIC, 2009).

Tapus and Mataric (2008) show an overview on Socially Assistive Robots (SAR) focusing on personality, empathy, physiological signals, and adaptation. On the other hand, Scassellati and Vázquez (2020) show how SAR can be used in infectious disease outbreaks.

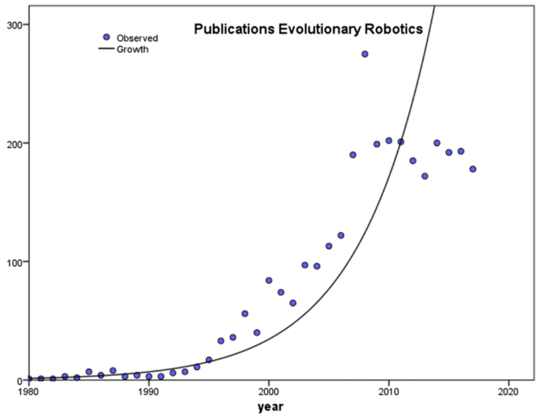

Figure 1 – Growth in the number of articles about 'robot' or 'robotics'

Source – Coccia (2018).

A possible definition and more information about SAR are presented by (FEIL-SEIFER; MATARIC, 2005). They show where SAR can be used, the research on SAR, and all their potential.

1.1 MOTIVATION

Based on the fact that children with ASD are stimulated when interacting with robots (SARTORATO; PRZYBYLOWSKI; SARKO, 2017), the Assistive Technology and Robotics Group (ATRG) at Federal University of Espirito Santo (UFES/Brazil) started a research project in 2013, whose goal was to develop a socially assistive robot for interaction with children with ASD (VALADÃO, 2016).

This Master's Dissertation presents an improvement for the robot created by ATRG through the use of *proxemic zones*, proposing a new control law to allow the robot to interact with children with ASD. Besides that, it is proposed here the introduction of concepts of *Workspace*, making the robot navigation limited by the acceptance of the child, since he/she can control the interaction staying inside or outside the interaction area. Moreover, there is a proposal for an internal representation of the robot emotional state and how this emotional state can be visualized as a robot's face. This last characteristic allows the robot to provide feedback to the child about the interaction in a natural way. Finally, this work makes the implementation easier to modify or to adapt by the incorporation of ROS[1].

1.2 STATE OF THE ART

In this section some studies applied on social robots are presented, such as how proxemics, emotions, and ROS in their implementation.

[1] A set of libraries and tools that makes an interface like an Operational System to help software developers create robot applications <https://wiki.ros.org>.

Figure 2 – Synthetic expressions for PEP value of happiness, surprise, anger, neutral, sadness, fear, and disgust, respectively from top left to bottom right

Source – Zhang et al. (2010).

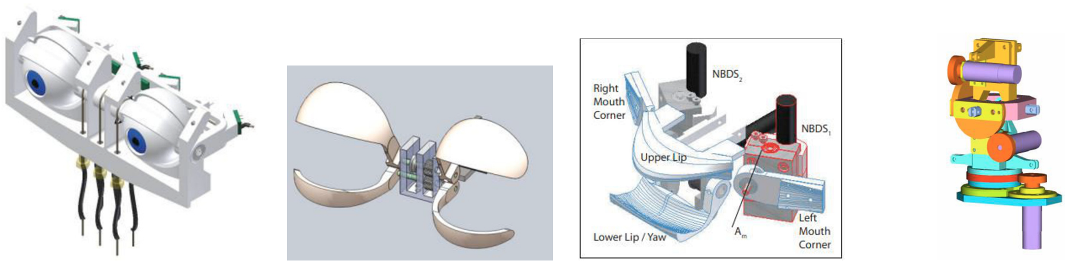

(a) Eyes System (b) Eyebrows (c) Mouth System (d) Neck System

Figure 3 – Mechatronics aspects and design concepts

Source – Adăscăliţei and Doroftei (2012).

1.2.1 Emotions in Social Robots

Can a robot express feelings? Robot emotional representation and expression can allow the robot to interact with a human in a more natural way, giving the same tips human do? These questions have motivated some studies.

Zhang et al. (2010) showed an affective talking avatar that uses three-dimensional pleasure-arousal-dominance (PAD) model to emulate facial expressions. They proposed a layer between Facial Animation Parameters (FAPs), better explained in Pardàs and Bonafonte (2002), and PAD, that allows emulating a Japanese Female Facial Expression using an Avatar. This layer, that was called Partial Expression Parameters (PEPs), can be represented using a mathematical function, and was used to create facial expressions, as shown in Figure 2.

Adăscăliţei and Doroftei (2012) showed an overview concerning the design solutions adopted in the development of a mechatronic that represents emotions of a social robot, using an eye system, with eyelids, eye-balls, and eyebrows; a mouth system, with upper lip, down lip, and a jaw; and a neck system, as shown in Figure 3.

Paiva, Leite and Ribeiro (2014) presented the importance of *Affective Loop* (represented on Figure 4) to stipulate the interaction between the robot and the human, and what is essential to exist in the construction of the robot. Affective interactions have some

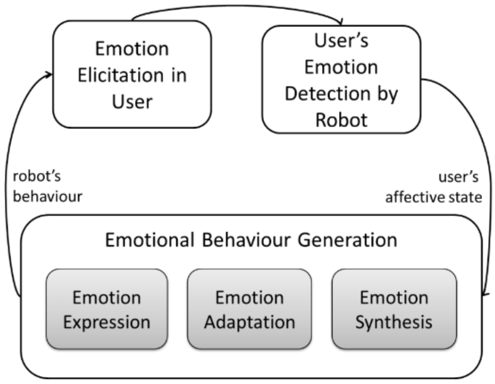

Figure 4 – Affective Loop of Emotional Robots

Source – Paiva, Leite and Ribeiro (2014).

purposes, among which stand out: to give the illusion of life, to augment engagement, and to augment social presence in the long-term. They also presented an overview on researches that use principles of animation for expressing emotions in robots and how the emotions can be computed. They addressed the SAIBA (Situation, Agent, Intention, Behavior, Animation) framework. According to them this framework has been used by various authors because BML (Behavior Markup Language, a part of SAIBA) contains a definition of that which the character has intended to do, contains the specific details about the manner in which the character is planning to perform its intention, and contains details on how the actual character will perform it.

Models used for representing emotions were researched by Kołakowska et al. (2015). Starting in the discrete representation model, passing through the dimensional (bi or three-dimensional) and Plutchik models, until reaching the Ortony, Clore, and Collins model (commonly referred to as the OCC model), they made a vast review of definitions, qualities and uses of each model. They also showed how these models can be used in applications.

Zhou and Shi (2017) proposed a novel method for facial expression synthesis, using Conditional Difference Adversarial Autoencoder (CDAAE) to model changes of low-level facial features. They showed also how this technique was used to create facial representations of emotions from a real face, as shown in Figure 5.

Paiva et al. (2018) studied how emotional processes are a main part in the creation of social robots. They showed examples of incorporating the concept of empathy in robotic tutors, examples of robots that share their emotions, and examples of robots that act as partners in group-based activities.

Chebotareva et al. (2019) developed a psycho-emotional system implementing four basic emotions using a spiking neural network based on Izhikevich model to 'decide' how to interact with the environment based on its psycho-emotional state. They proposed the

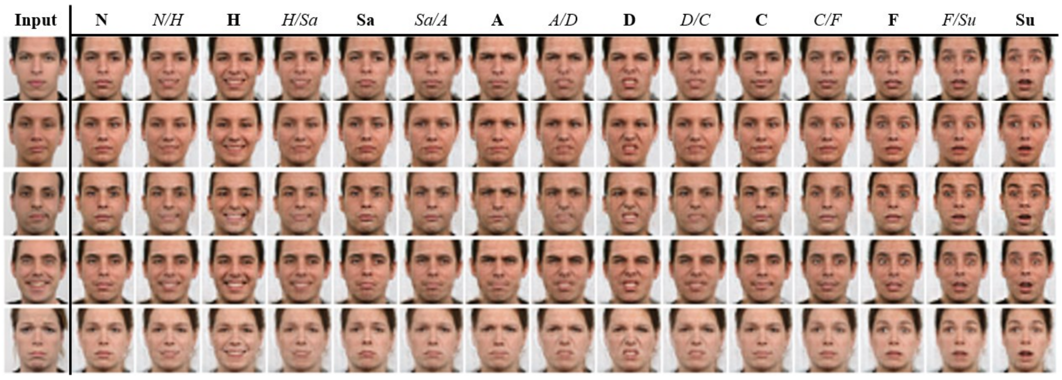

Figure 5 – Synthesis results of all the emotion classes and their interpolation using the CDAAE network (**N**eutral, H:happiness, Sa:sadness, A:anger, D:disgust, C:contempt, F:fear, Su:surprise). Each line presents one person with the original image at the input and all synthetic emotions

Source – Zhou and Shi (2017).

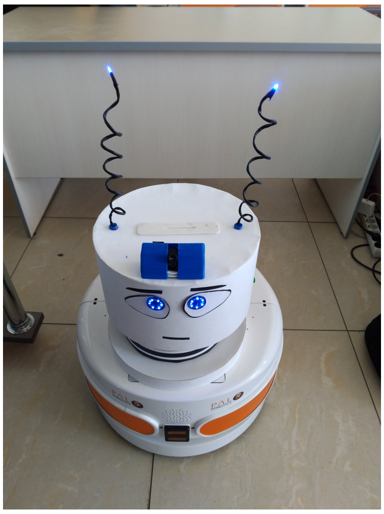

Figure 6 – High level design of the proposed system

Source – Chebotareva et al. (2019).

emotional social robot *Emotico* that shows emotions according to simultaneous stimuli of face detection and the introduction of coins. *Emotico* uses an adapted Hugo Lövheim's "cube of emotions" (LÖVHEIM, 2012) as basic emotional model for their robot based on two monoamines: dopamine (DA) and erotonin (5-hidroxitriptamina or 5-HT). The robot starts the protocol of interaction 'feeling sad' and drives to find a source of coins, because when the robot gets real coins its DA and 5-HT neuromodulators are increased. There are real and fake coins that can be used in interaction between human and the robot, which interfere in its emotions. If the robot gains a fake coin, only the 5-HT level increases, representing a disgust emotion. Their robot is shown in Figure 6.

Pena and Tanaka (2020) proposed an emotion representation using facial expressions (drawn in a LCD) and robot's body temperature, as shown in Figure 7. They showed that

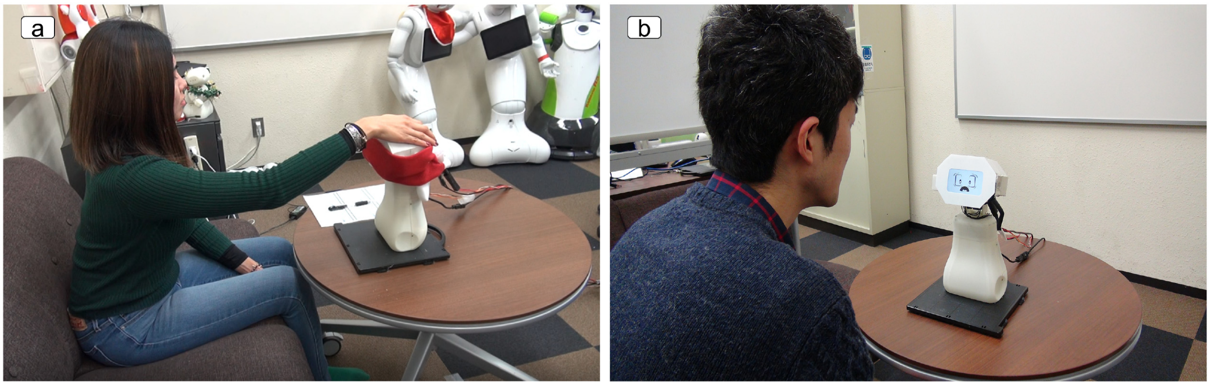

Figure 7 – Human Perception of Social Robot's Emotional States via (a) Thermal and (b) Facial Expressions

Source – Pena and Tanaka (2020).

facial expression influences more in relation to the perception of emotional state than thermal expression. And the combination of facial expression and thermal expression can generate four types of emotions: neutralized, in which the emotional state is avoided to be expressed; simulated, in which there is an emotional expression without feeling any emotional state; genuine, in which the emotional state is really expressed; and masked, in which the emotional state is covered by expressing a different emotional expression.

This work uses robot emotions, considering the relevance of and the great impact it has in the interaction with a human. Emotions are computed from the interaction of the robot with the child respecting Proxemics and the concept of *Workspace*. Here is proposed an internal representation for robot's emotions and its representation using a robot's face. Just as emotions, proxemics are very important in establishing trust and empathy, and also is used in this work.

1.2.2 Proxemics in Social Robots

Proxemics determines the relation with humans using the interpersonal distance. As it is an important concept, researchers are incorporating proxemics in the design of robot behaviors making them more acceptable for humans.

Walters et al. (2009) proposed an empirical framework that can be extended and that allows incorporating some effects, showing how the measurement and control of interpersonal distances between a human and a robot interfere in a proxemic behavior; and Takayama and Pantofaru (2009) showed how the robots can impact on proxemic behaviors in human-robot interaction.

Mumm and Mutlu (2011) showed the use of a physical and psychological distancing in human-robot interaction; on the other hand, Mead and Matarić (2017) researched about three categories of feature representations often used by computational models of proxemics and showed how the psycho-physical representation can be used to do a socially aware navigation based on interaction potential.

Vitiello et al. (2017) proposed an adaptable robot proxemic behavior with respect to the human users' personality and human actions using a neuro-fuzzy-Bayesian system; while Rösmann et al. (2017) showed a proposal of a novel motion model that predicts, plans and coordinates trajectories for social robot navigation respecting proxemic aspects; and Yeh et al. (2017) presented the use of proxemics in an interaction between a drone and a human.

Ginés et al. (2019) showed how dynamic proxemic zones can be used in a social navigation. Clavero et al. (2020) developed an adaptive proxemic zone using an asymmetric Gaussian function to represent different proxemic shapes based on the context information and using it to perform a social navigate task. And Ruijten and Cuijpers (2020) studied how the robot's approaching interferes in an interaction space shared by two people in a conversation.

This way, studying and using proxemics in social robots are fundamental to bring to the robot a more natural and acceptable behavior near to children with ASD, and, therefore, proxemics concepts are used in this work.

What justifies this work is the use of the concepts of proxemics, with the adition of *Workspace*, to propose a control law that allows and stimulates the approximation between the robot and the child. Unlike the studies presented earlier, which aimed at the displacement of the robot respecting the proxemics, but with the objective of not occurring collisions. In this work, in order to promote and stimulate an interaction using proxemics, there is an intention that the robot approaches and allows the touch in its structure.

1.3 OBJECTIVES

1.3.1 Main Objectives

The main goal of this Master's Dissertation is to make the robot demonstrate a friendly behavior, representing emotions and getting as close to the child as possible.

1.3.2 Specifics Objectives

The specifics objectives are:

- Incorporate ROS in the robot that is being developed by ATRG;
- Introduce the concept of *Workspace*;
- Define a new control law using proxemics concepts;
- Propose an emotion representation and how to simulate it.

1.4 STRUCTURE OF THE TEXT

This text is structured in five chapters. The first chapter has an introduction to the dissertation, presenting motivation, objectives and the state of the art.

The second chapter presents the concepts of emotions, proxemics and mobile robots that are the core of this work.

The third chapter contains a propose of representation of emotions, a implementation of the robot controller using ROS and how these things cooperate to reach the objective of make robot a social robot.

The fourth chapter presents simulations and results obtained.

And the last chapter shows the conclusion of this work and proposals for future works.

2 THEORETICAL BACKGROUND

> Where were you when I put the earth on its base? Say, if you have knowledge.
>
> Job, 38, 4

Some concepts are used in this Master's Dissertation and need to be reviewed. In next sections proposals of emotion's representation are presented, how the proxemics is defined and its use on social robotic, and finally the use of robots in social therapies.

2.1 EMOTIONS

Researchers define emotions as a systematic and complex psycho-physiological body response to behavior stimulus or to relationships (KOWALCZUK; CZUBENKO, 2016; MYERS, 2011; LAZARUS; LAZARUS, 1994; PLUTCHIK, 2001b).

There are many ways to classify and to represent emotions in order to differentiate between them, in special there are three major model types to represent emotions according to specialists: discrete, dimensional, and componential (KROUPI; YAZDANI; EBRAHIMI, 2011; KOŁAKOWSKA et al., 2015; COPPIN; SANDER, 2013; PHAN; SHINDO; MATSUMOTO, 2016). These representations are better explained in the next sections.

2.1.1 Emotion representation

Some authors affirm that, independently of races, ages, behavior, environment, experiences, there are a finite number of discrete emotions that represents the variety of beliefs (EKMAN; FRIESEN, 1971; MARCUS, 2003). Specially, Ekman and Friesen (1971) proposed that there are six basic mutually exclusive emotions called anger, disgust, fear, happiness, sadness, and surprise (shown on Figure 8).

Although these basic emotions are used in different studies and have simple comprehensibility for human, they can not describe all emotions and its variants. Therefore, the research proposed the use of dimensional models to represent various emotions (SCHERER, 2013; RUSSELL, 1980; KUPPENS et al., 2013; PREOŢIUC-PIETRO et al., 2016). On 1980, Russell (1980) introduced the concept of *Circumplex Model*, in which a particular emotion is a linear combination of two independent neurophysiological systems (represented in a two-dimensional space): valence and arousal. In Figure 9 a graphical representation of the circumplex model of affect is shown, where the horizontal axis represents the valence dimen-

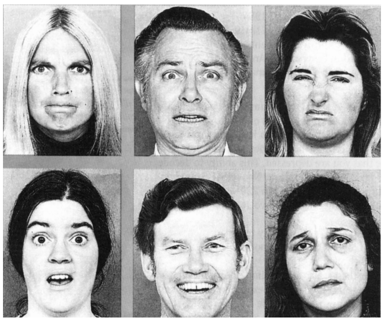

Figure 8 – Six basic emotions. On the top, from left to right: anger, fear, and disgust. On the bottom, from left to right: surprise, happiness, and sadness

Source – Ekman and Friesen (1971).

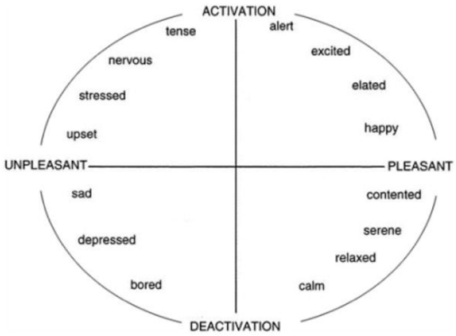

Figure 9 – A graphical representation of circumplex model

Source – Posner, Russell and Peterson (2005).

sion and the vertical axis represents the arousal or activation dimension. The *Circumplex Model* has some disadvantages: people do not think about emotions as points; ambivalent emotional states are hard to be represented; and fear and anger are indistinguishable, because these emotions both lie in the same quadrant of high arousal and negative valence (KOŁAKOWSKA et al., 2015). To solve these questions an addition of a third dimension was proposed. One of the 3D models most popular is Pleasure-Arousal-Dominance (PAD), shown on Figure 10, proposed by Mehrabian and Russell (1974), where pleasure dimension corresponds to valence in *Circumplex Model*, arousal has the same propose, and dominance represents a reaction to stimuli. Therefore, it is possible to differentiate anger from fear (according to as shown in Figure 11).

In 1980 (PLUTCHIK, 1980) introduced a componential model type to represent emotions, proposing two taxonomic categories: primary (basic) and complex (combinations of primary emotions). Using a parallel with colors, he showed a concept of *Wheel of Emotions*, which has eight basic emotions (joy, trust, fear, surprise, sadness, disgust, anger, and anticipation) with three intensity degrees each (attenuated, basic, or extrapolated). The intensity of emotion increases towards the center of the wheel and decreases in the other direction.

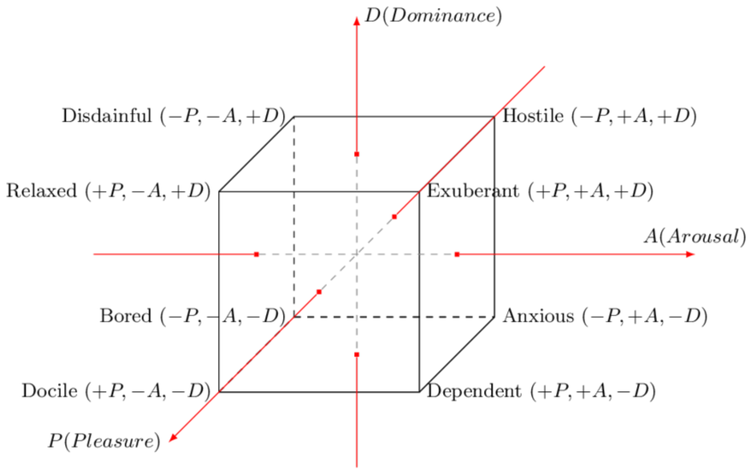

Figure 10 – Pleasure-Arousal-Dominance graphical representation

Source – Tarasenko (2010).

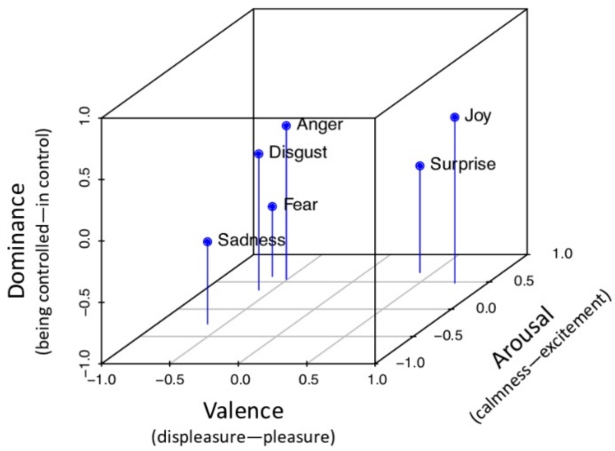

Figure 11 – PAD: How the addition of *Dominance* dimension permits to differentiate anger from fear

Source – Feidakis et al. (2019).

Figure 12a shows the wheel of emotions proposed by him and a 3D representation of this wheel.

He defined relationship of two emotions according to their spatial displacement in wheel of emotions, where a *dyad* is a complex emotion raised when two emotions are elicited together. There are primary, secondary, tertiary and opposite dyads. Primary dyad, representing often felt emotions, occurs when two adjacent emotions are triggered (for example, when joy and trust are triggered together, love is raised). Secondary dyad, representing sometimes felt emotions, occurs when two emotions that are two petals away are triggered (for example, joy and fear, raising guilt). Tertiary dyad, representing seldom felt emotions, occurs when two emotions that are three petals away are triggered (for example, joy and surprise, raising delight) Finally, opposites dyads, representing conflicts, occurs when opposite emotions are triggered (for example, joy and sadness, raising a

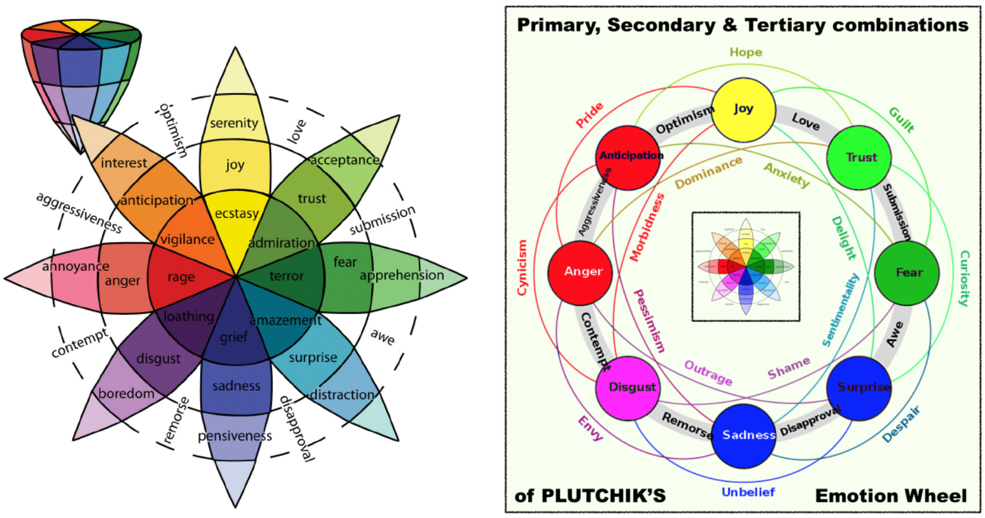

(a) Wheel of emotions (b) Combination of emotions

Figure 12 – Wheel of emotions and how these emotions can be mixed

Source – (a) Plutchik (2001b), (b) Torbico (2011).

conflict) (KOŁAKOWSKA et al., 2015; SEMERARO; VILELLA; RUFFO, 2021; CHEN; LEE; HUANG, 2011).

These combinations (primary dyad, secondary dyad, and tertiary diad) are represented as links in Figure 12b (TORBICO, 2011).

2.1.2 Mathematical Model

Using the concept introduced by (PLUTCHIK, 2001b), Rodrigues, Asla and Velho (2009) presented a mathematical model, called *Emotion Hypercube*, to represent emotions and their variations, in which an emotion is represented using a vector with four dimensions.

They defined a *family of emotions*, denoted by F_i, as a set of different intensity levels of a basic emotion E_i. There are eight *family of emotions*, with three levels of intensities (attenuated, basic, and extrapolated). The basic emotion gives the name to the family:

Joy's family : $F_{\text{joy}} = \{\text{serenity, joy, ecstasy}\}$;

Sadness's family : $F_{\text{sadness}} = \{\text{pensiveness, sadness, grief}\}$;

Trust's family : $F_{\text{trust}} = \{\text{acceptance, trust, admiration}\}$;

Disgust's family : $F_{\text{disgust}} = \{\text{boredom, disgust, loathing}\}$;

Fear's family : $F_{\text{fear}} = \{\text{apprehension, fear, terror}\}$;

Anger's family : $F_{\text{anger}} = \{\text{annoyance, anger, rage}\}$;

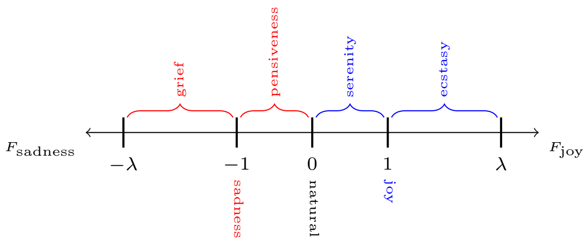

Figure 13 – Graphical representation of the x axis

Source – By author, adapted from Rodrigues, Asla and Velho (2009).

Surprise's family : F_{surprise} ={distraction, surprise, amazement}; and

Anticipation's family : $F_{\text{anticipation}}$ ={interest, anticipation, vigilance}.

Using the definition of *family of emotions* they proposed the concept of *emotion axis*, which is constituted of a pair of opposite family emotions (according to Plutchik). The intensity level for an emotion E_e on the e axis is represented by a real value $\alpha_e \in [-\gamma, +\gamma]$, with $\gamma \geq 1$. Therefore, the basic emotion of the family is map to $+1$ ($\alpha_e = 1$), the basic emotion of its opposite family is map to -1 ($\alpha_e = -1$), and the absence of emotion is mapped to zero ($\alpha_e = 0$). Emotions with intensity $|\alpha_e| > 1$ are considered as an extrapolation of a basic emotion, while emotions with intensity $0 < |\alpha_e| < 1$ are considered as an attenuation of a basic emotion.

From this, they proposed four axes:

x : positive semi-axis to represent F_{joy}, and negative semi-axis to represent F_{sadness};

y : positive semi-axis to represent F_{fear}, and negative semi-axis to represent F_{anger};

z : positive semi-axis to represent F_{trust}, and negative semi-axis to represent F_{disgust}; and

w : positive semi-axis to represent $F_{\text{anticipation}}$, and negative semi-axis to represent F_{surprise}.

Figure 13 shows a graphical representation of the x axis.

In this Master's Dissertation an adaptation of this *Emotion Hypercube* is used as will be presented in Section 3.2.

2.2 NON-VERBAL COMMUNICATION

Communication is an important instrument in our society, which can be used to interact, instruct, show an emotion, or even dominate (NARVARTE, 2014). It is divided in two areas: verbal and non-verbal and is expressed in many ways (MAVRIDIS, 2015) like as interactions peer to peer or as a specialized language (BEREA, 2019).

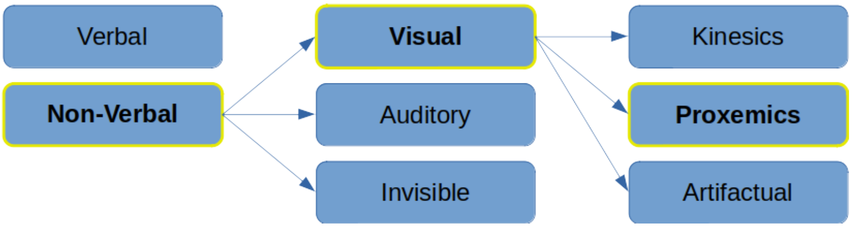

Figure 14 – Verbal and Non-verbal Communication Systems

Source – By author.

Non-verbal communication was defined by Leathers and Eaves (2016) as the use of interacting sets of visual, vocal, and invisible communication systems and subsystems by communicators with the systematic encoding and decoding of non-verbal symbols and signs for the purpose(s) of exchanging consensual meanings in specific communicative context. In the Figure 14 is shown how authors represent the interacting communication systems.

These researchers also showed that non-verbal communication comprises three major interacting systems: the visual communication system, the auditory communication system, and the invisible communication system. According to them, visual communication system is the most important because it is made of extremely important subsystems: kinesic (how body movements are interpreted), proxemics (how one feels about the presence of other person in his/her personal space), and artifactual communication (how objects can be used to convey messages) (LEATHERS; EAVES, 2016).

Non-verbal communication is used in robotics to create a channel of interaction with humans, specially when trying to create a proximity with them.

2.2.1 Proxemics

Proxemics is the study of non-verbal communication according to the individual use of space, distance and orientation, in various social and interpersonal situations (RIOS-MARTINEZ; SPALANZANI; LAUGIER, 2015; HALL, 1966).

Regarding social distances, studies conducted by Hall (1966) observed the existence of certain unwritten rules that lead individuals to maintain distances from others, and lead others to respect this distance (RIOS-MARTINEZ; SPALANZANI; LAUGIER, 2015).

Rios-Martinez, Spalanzani and Laugier (2015) defined *personal space* as a region stipulated by a person around himself/herself to not cause discomfort to others when establishing interaction. They showed that there are some shapes to represent personal space: concentric circles, egg shape (bigger in the front), ellipse shape, and shape smaller in the dominant side (see Figure 15 for more details). Egg shape and ellipse shape are most used by researchers to represent an interaction between a robot and a human when

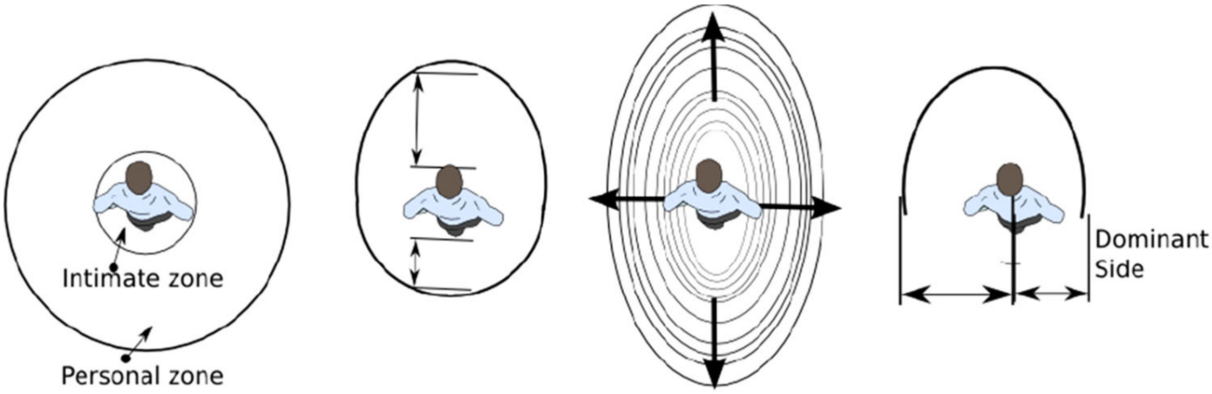

Figure 15 – Different shapes of personal space

Source – Rios-Martinez, Spalanzani and Laugier (2015).

there is interest to avoid interaction, for example are used to represent human obstacles (HERRERA et al., 2019; BARNAUD et al., 2014), walking motion (RATSAMEE et al., 2013), or human following (HERRERA et al., 2017). On the other hand, concentric circles is most used when there is interest to have interaction (MEAD; MATARIĆ, 2017; GINÉS et al., 2019).

About concentric circles, Rios-Martinez, Spalanzani and Laugier (2015) classify personal space in four specific zones:

public zone : $d > 3.6\,\mathrm{m}$;

social zone : $d > 1.2\,\mathrm{m}$;

personal zone : $d > 0.45\,\mathrm{m}$;

intimate zone : $d \leq 0.45\,\mathrm{m}$.

where d is the distance between humans.

This Master's Dissertation uses the same four zones, changing the name of *intimate zone* to *security zone*, just to reinforce what will be the use of this zone. Values are adapted to facilitate simulations and were determined empirically:

public zone : $d > 3.75\,\mathrm{m}$;

social zone : $d > 1.75\,\mathrm{m}$;

personal zone : $d > 0.5\,\mathrm{m}$;

security zone : $d \leq 0.5\,\mathrm{m}$.

In this case d represents the distance between the robot and a child.

How these zones interfere in robot movements is more detailed in Section 3.3.4.

2.3 ROBOTIC

Robots are intrinsically linked to recent human history. In industry, medicine, or even music, the use of robots is increasingly noticed (HOCKSTEIN et al., 2007; KAPUR, 2005).

They can be pre-programmed (that operate in a controlled environment where they do simple, monotonous tasks, like a mechanical arm on an automotive assembly line), humanoid (that look like and/or mimic human behavior), autonomous (that operate independently of human operators, like a robot vacuum cleaner), teleoperated (that are semi-autonomous bots that use a wireless network to enable human control from a safe distance, like Remotely Operated Underwater Vehicle), or to rehabilitation (that either enhance current human capabilities or replace the capabilities a human may have lost) (DALEY et al., 2021; ROBOTS. . . , 2012). Figure 16 shows examples of each type of robot.

2.3.1 Mobile robots

Mobile robots are robots that have own movements under their control (Section 2.3). So, how they control their locomotion is an important aspect. They can walk, roll, run, or fly, and according to their locomotion system they can be classified as: stationary, land-based, air-based, or water-bases (RUBIO; VALERO; LLOPIS-ALBERT, 2019).

Wheeled mobile robot is a specific type of land-based mobile robot that uses a determined number of wheels to allow the robot to move. Wheeled robots can be classified according to drive system as: differential drive, car-like, omnidirectional, or synchro drive (RUBIO; VALERO; LLOPIS-ALBERT, 2019).

A mobile robot with two-wheeled drive using differential steering and a free balancing wheel is the most common structure used to build a mobile robot (MALU; MAJUMDAR, 2014). It can be represented using an abstract model like shown in Figure 17, where the body of the robot is represented as a beige circle, its two driving wheels are represented using two tan rounded rectangles, the free wheel is represented as a gray circle, and the laser distance sensor is represented using a pale-green circle. The center of laser distance sensor is concentric with the middle of robot structure (viewing from the top). The front of robot is on axis X^R.

A special concept adopted in mobile robots is *pose*, which contains data about localization of the robot in an ambient. In this Master's Dissertation *pose* is defined as a vector $\vec{\xi} = \begin{bmatrix} x & y & \psi \end{bmatrix}^\mathrm{T}$ where x and y are the Cartesian positions of the robot in a global reference $\langle O^W, X^W, Y^W \rangle$, and ψ is the angle between the robot's front and X^W axis.

Adopting unicycle robot (for more details, please read Lee et al. (2001)) as an abstraction of the real robot, it is possible to represent robot's movements using the

(a) Pre-programmed

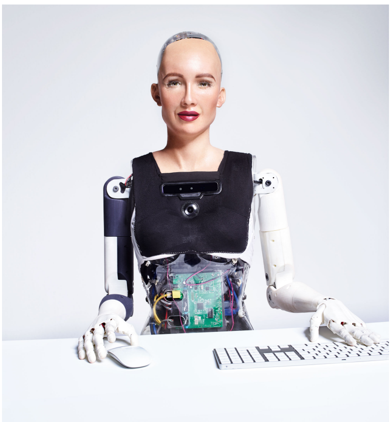

(b) Humanoid

(c) Teleoperated

(d) Autonomous

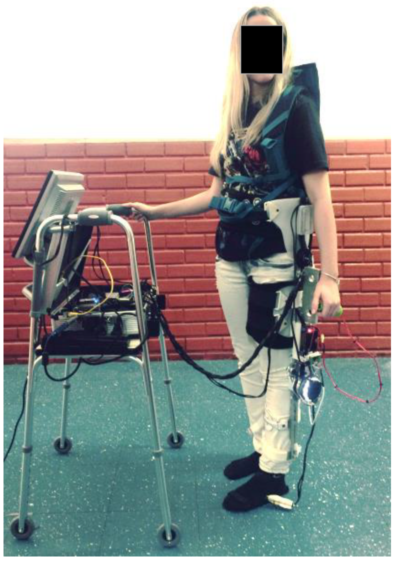

(e) Augmenting

Figure 16 – Examples of types of robots

Source – (a) Tsarouchi et al. (2014), (b) Hanson Robotics (2021), (c) Nogueira (2017), (d) Prassler et al. (2000), and (e) Parra (2017).

cinematic model:

$$\begin{aligned}\dot{x} &= v\cos\psi \\ \dot{y} &= v\sin\psi \\ \dot{\psi} &= \omega\end{aligned} \tag{2.1}$$

and adopting polar coordinates with error distance ρ, the same way position of robot can be represented as:

$$\begin{aligned}\dot{\rho} &= -v\cos\psi \\ \dot{\psi} &= -\omega + \frac{v\sin\psi}{\rho}\end{aligned} \tag{2.2}$$

where v is the linear velocity of the robot, and ω is its angular velocity. Figure 18 shows robot's initial position, where the robot's front (represented by its own axis X^R)

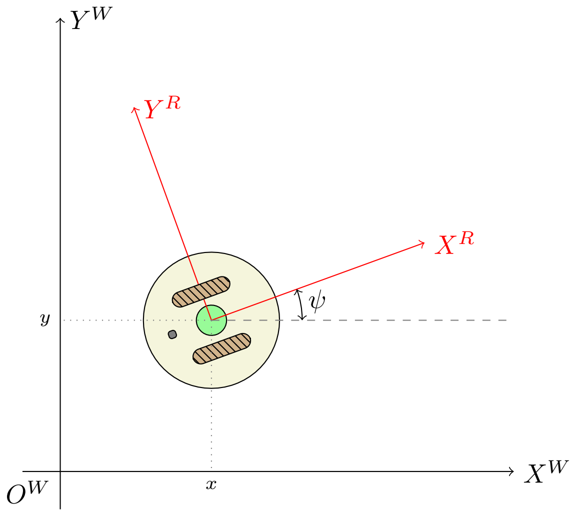

Figure 17 – Representation of a robot on a Cartesian coordinate system

Source – By author.

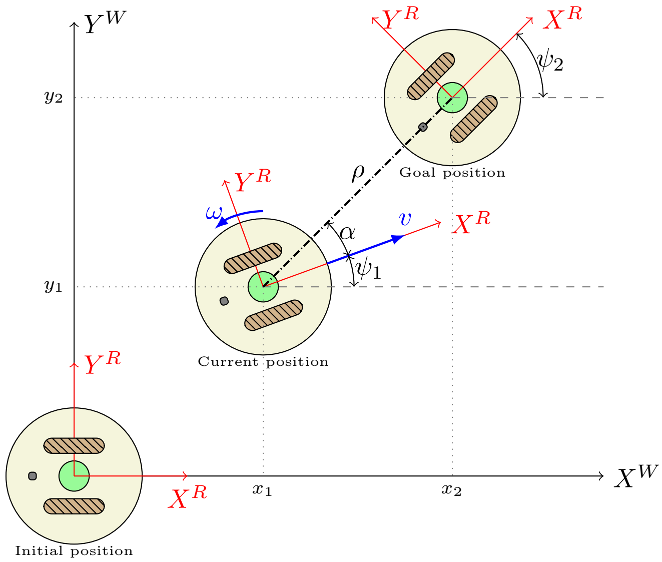

Figure 18 – Robot movements

Source – By author.

is coincident with global axis X^W. After some time, the robot is at current position $\vec{\xi_1} = \begin{bmatrix} x_1 & y_1 & \psi_1 \end{bmatrix}^\intercal$. The objective could be, for example, to move the robot to goal position $\vec{\xi_2} = \begin{bmatrix} x_2 & y_2 & \psi_2 \end{bmatrix}^\intercal$. Therefore, the robot receives commands of linear and angular velocities, v and ω, respectively, to achieve this objective; these is the same that doing $\rho \to 0$ and $\alpha \to 0$.

2.3.2 Social robots

Social robots play several important roles and benefits in the therapy of children with ASD. Whether using games or engagement activities, the robots stimulate the children to train their skills, to perfect their behaviors and to provide encouragement and positive feedback when successfully complete a task (CABIBIHAN et al., 2013; DIEHL et al., 2012).

They can be used to diagnosis, to elicit a behavior, or as a social mediator (to facilitate children with ASD's learning of some social rules (ZHANG et al., 2019), or improving social skills (SCASSELLATI et al., 2018)), or a friendly playmate, and mainly as a personal therapist (for example, teaching music (TAHERI et al., 2016)), because robots are less complex and less intimidating than humans, and make embodied interactions possible (CABIBIHAN et al., 2013).

2.3.3 Mobile social robots

There are some studies showing the use of mobile social robots. Vervisch et al. (2018) shows a do-it-yourself expansion kit that enables and facilitates the creation of mobile social robots. Satake et al. (2019) proposes a simulator that allows the simulation of interactions among people, and interactions between people and the robot. Finally, Hollinger et al. (2006) develops a social mobile robot using emotion-based decision mechanisms.

The first version for the robot, created by the Assistive Technology Group at Federal University of Espirito Santo (UFES/Brazil), was termed `MARIA` (Mobile Autonomous Robot for Interaction with Autistics), which had some human features, but looking more like with a toy than a human. `MARIA` had two embedded behaviors: self-presentation and play. This robot got promising results, but presented some limitations (VALADÃO, 2016), which motivated the development of a new version. In the second version (termed `New-MARIA` or `N-MARIA`) a dynamic face, touch sensors, ability for identification of children around itself (i.e. detection in 360°), and a set of cameras to infer emotions of the children were incorporated to the robot. Some robot's features were also changed, such as: all robot structure was segmented to facilitate its transportation; soft materials were used for children safety; and its external structure had anthropomorphic features now (BINOTTE, 2018). Figure 19 shows the first version (on the left) and the second version (on the right) of the robot `MARIA`. For more details on the robot design, please read (VALADÃO, 2016; BINOTTE, 2018).

Observing the difficulty to transport the second version of `MARIA` and, because that, the limited number of assisted children, and wanting to add new functionalities as application in therapies also with children with Down Syndrome using serious games, a new version of the robot `MARIA`, called `MARIA-T21`, was proposed by (PANCERI et al., 2020). Figure 20 shows the proposed model of the new version (on the left) and the robot that was made (on the right). Results of this Master's Dissertation will be used in this new version, that is in development.

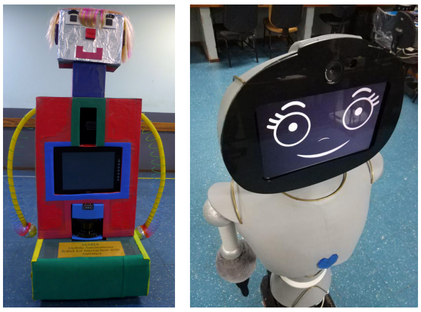

Figure 19 – Versions of Mobile Autonomous Robot for Interaction with Autistics (`MARIA`), the first (left) and the second (right) versions of the robot

Source – Piero, Caldeira and Bastos Filho (2020).

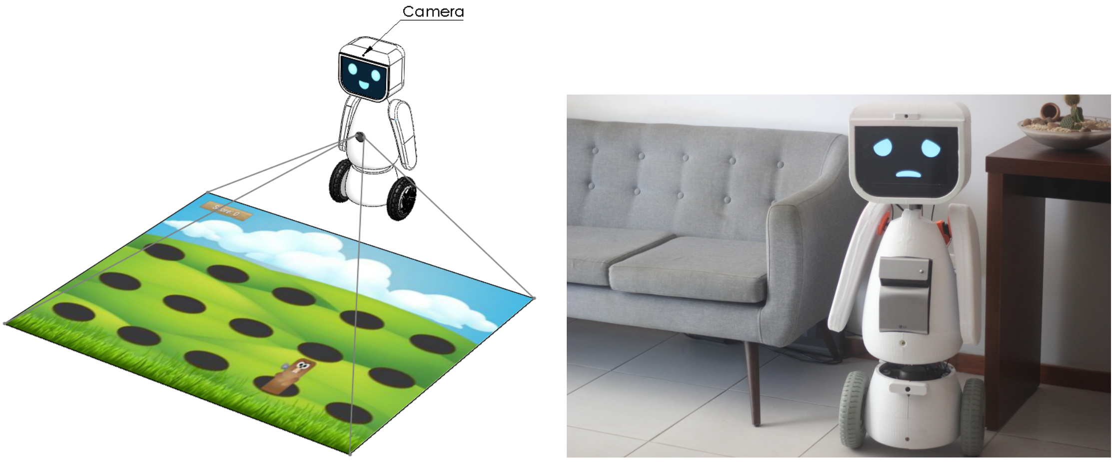

Figure 20 – `MARIA-T21`

Source – Panceri et al. (2020).

2.3.4 Robot Operating System

In order to provide a software structure allowing aggregating new behaviors and modify old ones, in the project of `MARIA-T21` all systems are being implemented using Robot Operating System (ROS).

ROS is a free collection of software libraries of programs and tools to serve as a common software platform, as a framework, to access and control robotic systems, allowing a distributed and modular design for people who are building and using robots (KERR; NICKELS, 2012; CASHMORE et al., 2015; QUIGLEY; GERKEY; SMART, 2015).

ROS is being used in the `MARIA-T21` project because it is thin, has a clean functional interface, is language independent (C++, Java, Python can be used to create programs), allows easy testing, and is scalable (DATTALO, 2018). Using ROS, some concepts are necessaries: a node is a running instance of a program that uses interface to communicate with other nodes. A message is a structured data shared between nodes, and a topic is where these data are published or obtained. A special node called Master provides all structure necessary to correct functionality of the rest of the nodes (ROBERT, 2020).

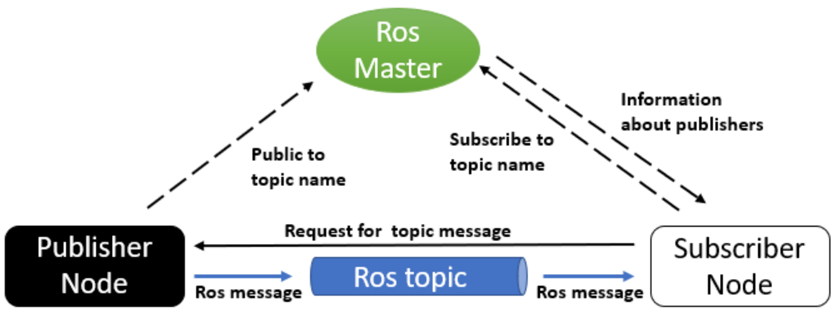

Figure 21 – Concepts used on ROS: *node*, *topic*, *message*, *master*

Source – Robert (2020).

Figure 21 shows a representation of nodes, topic, and messages.

This chapter has presented a part of theoretical background about emotions, robotics, and proxemics. Some others concepts can be obtained in referenced documents. In special, in the next chapter the concepts of wheeled mobile robots, proxemics, and Plutchick representation of emotion will be shown.

3 DEVELOPMENT

Nevertheless I must walk to day,
and tomorrow, and the day
following: for it cannot be that a
prophet perish out of Jerusalem.

Luke, 13, 33

In order to promote a better and more natural interaction between the robot and the child, in this work it is developed a behavior that allows the robot to stay near to the child using proxemics concepts to be socially accepted by the child, not scaring him/her or compromising his/her safety.

Therefore, this chapter presents the control system development that will be used in `MARIA-T21`. It starts showing some definitions made to guide the controller like *Work Area* (which defines area where there is interaction between the robot and the child, and area where the child can move to avoid this interaction) and *Emotion Hypercube* (adapted from Rodrigues, Asla and Velho (2009)) to represent the robot emotional state in response to the interaction realized with the child. In the sequence, implementation using ROS of all parts of the system are shown, including linear and angular velocities controller implemented to move the robot when it is required, child detection using laser sensor, and the control of the emotional state of the robot based on the proxemics concepts of interaction.

3.1 WORK AREA

The robot works in a plane delimited area where it can move in all directions. There are two basic movements: linear velocity, v; and angular velocity, ω. A positive linear velocity, $+v$, makes the robot to go forward, and a negative linear velocity,$-v$, makes it to go backward. A positive angular velocity, $+\omega$, makes the robot to rotate anti-clockwise, and a negative angular velocity, $-\omega$, makes the robot to rotate clockwise.

To detect people or obstacles the robot uses a Light Detection And Ranging (LiDAR) sensor developed by SLAMTEC[1] called RPLIDAR A1, that measures range from 0.15 m to 12 m, angles range between 0° and 360°; it has a measurement resolution less than 0.5 mm, and an angular resolution of 0.9°, and reads a single measurement each 0.25 ms. The LiDAR sensor is positioned in the rotate center of the robot and realizes measures according to a referential with axis x pointing in the same direction the robot

1 <https://www.slamtec.com/en/Lidar/A2>

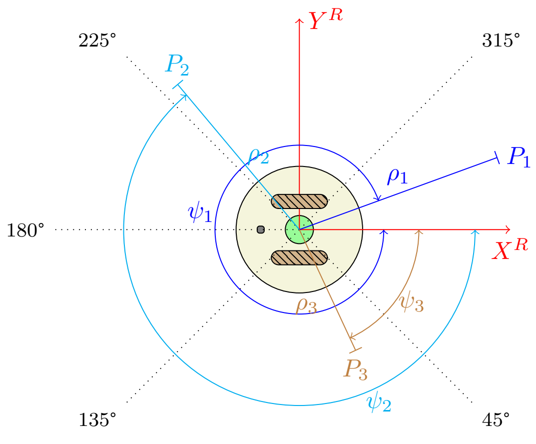

(a) RPLIDAR A1 representation

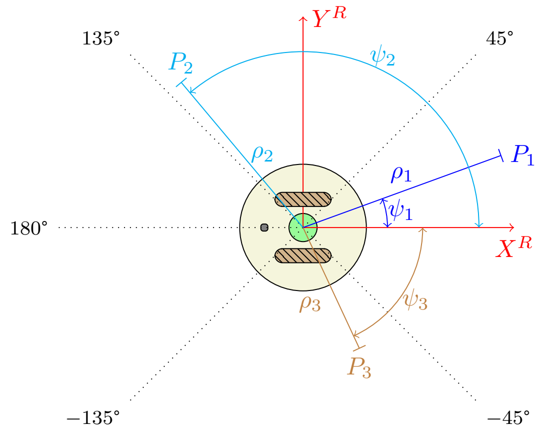

(b) Robot representation

Figure 22 – Mapping from RPLIDAR A1 representation to Robot representation

Source – By author.

Table 1 – Examples of points in RPLIDAR A1 representation and Robot representation

Point	RPLIDAR A1 representation	Robot representation
$P_1 = \langle \rho_1, \psi_1 \rangle$	$\langle 3\,\text{m}, 340° \rangle$	$\langle 3\,\text{m}, 20° \rangle$
$P_2 = \langle \rho_2, \psi_2 \rangle$	$\langle 2.7\,\text{m}, 230° \rangle$	$\langle 2.7\,\text{m}, 130° \rangle$
$P_3 = \langle \rho_3, \psi_3 \rangle$	$\langle 1.9\,\text{m}, 65° \rangle$	$\langle 1.9\,\text{m}, -65° \rangle$

Source – By author.

moves with positive linear velocity. The rotation angle increases as rotating clockwise, starting at axis x. During the working process, it outputs a set of 360 samples, a sample for each angle from 0° to 360°.

As showing in Figure 22a, RPLIDAR A1 data contains a pair of values, $\langle \rho_i, \psi_i \rangle$, that represents, in polar coordinates, the distance of the robot's center to the obstacle (or person), and the angle where this obstacle is, respectively. On the other hand, Figure 22b shows how the robot represents these points in the robot referencial system using polar coordinates too. To exemplify, Table 1 shows how three points $\{P_1, P_2, P_3\}$ are represented in the two forms, using RPLIDAR A1 representation and Robot representation. Observing distances ρ_i it is possible to infer that there are no differences in two representations. However, it is necessary to define how an angle ψ from RPLIDAR A1 representation is mapped to another angle ψ' in Robot representation. To do that, an adjustAngle(ψ) function is defined:

$$\psi' = \text{adjustAngle}(\psi) = \begin{cases} -\psi, & 0° \leq \psi < 180° \\ 360° - \psi, & 180° \leq \psi < 359° \end{cases} \tag{3.1}$$

Considering the comfort and safety of the child, in this Master's Dissertation an area of interaction with predefined form and dimensions is defined. If the child wants to interact with the robot, he/she shall be inside this area and if the child is outside the interaction area, the robot infers that the child does not want interaction. This idea, used in Binotte (2018), allows an interaction with the child avoiding any trauma related to the robot approximation, respecting the child's will and time to interact.

Therefore, the protocol adopted here for simulation stipulates a plane rectangle area, called *Workspace*, with 14 m in one side (axis x) and 12 m in other side (axis y). The robot starts the simulation in the middle of the *Workspace* and this point is the world referential for all the experiments.

The *Workspace* has some special areas: *internal*, *observation*, and *external*, defined according to Equation 3.2:

$$\mathrm{wsp}(x,y) = \begin{cases} \text{internal} & |x| < X_{\text{int}} \text{ and } |y| < Y_{\text{int}} \\ \text{observation} & X_{\text{int}} \leq |x| \leq X_{\text{ext}} \text{ and } Y_{\text{int}} \leq |y| \leq Y_{\text{ext}} \\ \text{external} & |x| > X_{\text{ext}} \text{ or } |y| > Y_{\text{ext}} \end{cases} \tag{3.2}$$

where (x, y) is the position on the space reached by the robot (x and y are given in meters in global reference $\langle O^W, X^W, Y^W \rangle$, $X_{\text{int}} < X_{\text{ext}} \leq 7\,\text{m}$ and $Y_{\text{int}} < Y_{\text{ext}} \leq 6\,\text{m}$. Figure 23 shows the robot and the child (both represented as points, disregarding its size to simplify) in the *Workspace* representing *internal* as a white area, *observation* as a light gray area, and *external* as a dark gray area. In this figure, d_o is the distance of observation, d_i is the desired distance, and d_1, d_2, and d_3 are examples of distances that will be reduced to zero, according to where the child is on *Workspace*, considering that the robot objective is to be as close as possible to the child considering proxemics rules. The circle in turn of the robot represents the limit of distance to the child indicated by the *promexic zone* in which the robot is, so the robot aims to stay at this distance to the child in order to have the maximum interaction possible.

The robot has special actions according to child's position in the *Workspace*. Figure 23 shows three possible positions of the child during the interaction with the robot, and respective actions associated with them. In the first case, the child is in the *external area*, in which there will be no actions by the robot aiming to reduce d_1. In the second case, the child is in the *observation area*, so the robot will respect the boundary of the *internal area*, disregarding the distance the child has in the *observation area* (called, in this work, distance of observation d_o), and will monitor the movement of the child, always keeping itself 'looking' at the child keeping the child in its heading direction and reducing the distance d_2 to zero. Otherwise, the child is in the *internal area*, in which the robot will try to maintain an interaction based on concepts of *proxemic zones* proposed by (HALL, 1966), using a specific control law to approach, slowly, to the child, i.e. reducing the distance d_3 to zero.

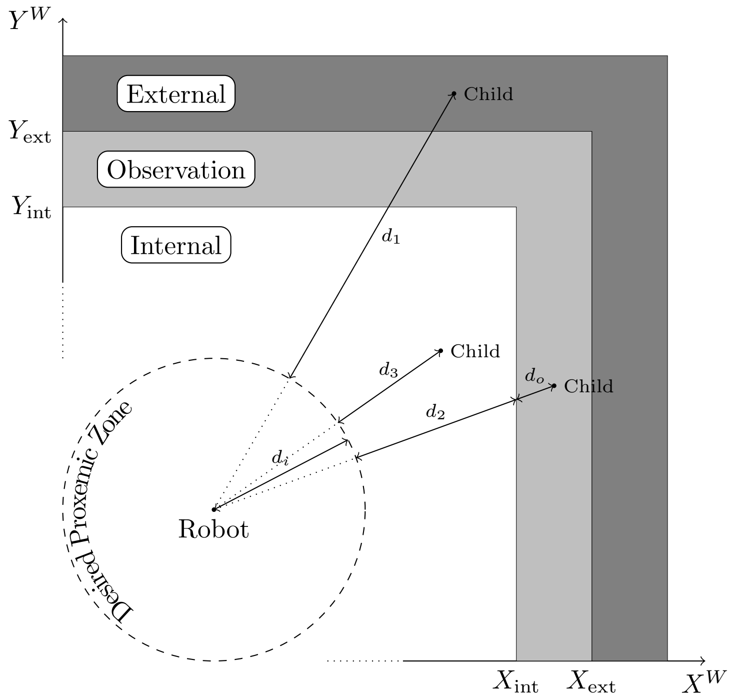

Figure 23 – Representation of *Workspace*

Source – Piero, Caldeira and Bastos Filho (2020).

3.2 ROBOT EMOTIONAL STATE REPRESENTATION

Due to the difficulty in the children with ASD to understand other emotions, in this work it is proposed that the robot manifests or presents its emotional state.

In order to give meaning to this emotional state it is proposed that the robot becomes happier when the child accepts its approximation and sadder when the child run away for the robot indicating that he/she is rejecting the robot.

However, before presenting at the robot face its emotion, it is necessary to have a way to represent its emotional state, changing it according to the proxemics interaction proposed.

So in this Master's Dissertation, the robot emotional state is represented using an adapted version of the system proposed by Rodrigues, Asla and Velho (2009). Here, it is adopted that:

x : positive semi-axis to represent F_{joy}, and negative semi-axis to represent F_{sadness};

y : positive semi-axis to represent F_{trust}, and negative semi-axis to represent F_{disgust};

z : positive semi-axis to represent F_{fear}, and negative semi-axis to represent F_{anger}; and

w : positive semi-axis to represent $F_{\text{anticipation}}$, and negative semi-axis to represent F_{surprise}.

Comparing with the representation proposed by Rodrigues, Asla and Velho (2009), axes y and z are exchanged and axis w is in the opposite direction.

Defining a canonical base $\mathcal{B} = \{\vec{e}_x, \vec{e}_y, \vec{e}_z, \vec{e}_w\}$ where:

$$\begin{aligned}
\vec{e}_x &= \begin{bmatrix}1 & 0 & 0 & 0\end{bmatrix}^{\mathtt{T}}, \\
\vec{e}_y &= \begin{bmatrix}0 & 1 & 0 & 0\end{bmatrix}^{\mathtt{T}}, \\
\vec{e}_z &= \begin{bmatrix}0 & 0 & 1 & 0\end{bmatrix}^{\mathtt{T}}, \text{ and} \\
\vec{e}_w &= \begin{bmatrix}0 & 0 & 0 & 1\end{bmatrix}^{\mathtt{T}}.
\end{aligned}$$

it is possible to represent an emotion as a vector $\vec{v}$ in the base $\mathcal{B}$,

$$\vec{v} = \begin{bmatrix}\alpha_x & \alpha_y & \alpha_z & \alpha_w\end{bmatrix}^{\mathtt{T}},$$

where $\alpha_x, \alpha_y, \alpha_z, \alpha_w \in \{x \in \mathbb{N} \mid |x| \leq 100\}$.

The intensity of an emotion $\vec{v} = \begin{bmatrix}\alpha_x & \alpha_y & \alpha_z & \alpha_w\end{bmatrix}^{\mathtt{T}}$ is calculated using Equation 3.3:

$$|\vec{v}| = \min\left\{\sqrt{\alpha_x^2 + \alpha_y^2 + \alpha_z^2 + \alpha_w^2}, 100\right\} \tag{3.3}$$

As mentioned in Chapter 2, Plutchik (2001b) and Rodrigues, Asla and Velho (2009) have considered three distinct levels of an emotion: *attenuated*, *basic*, and *extrapolated*; and a fourth level, called *neutral* or *natural* to represent absence of emotion. To map all values of an intensity of emotion, calculated using $|\vec{v}|$, into the set of distinct levels, the function $\mathrm{mapToLevels}(\vec{v})$ is defined as:

$$\mathrm{mapToLevels}(\vec{v}) = \begin{cases} \text{neutral}, & |\vec{v}| \leq 10 \\ \text{attenuated}, & 10 < |\vec{v}| \leq 40 \\ \text{basic}, & 40 < |\vec{v}| \leq 70 \\ \text{extrapolated}, & 70 < |\vec{v}| \leq 100 \end{cases} \tag{3.4}$$

Figure 24 shows a graphical representation of the x axis using $\mathrm{mapToLevels}(\vec{v})$ function to map natural values into family of emotions' discrete values. The semi-axes were divided into three segments of the same size, distributing in a more balanced way each emotion on semi-axes.

Phan, Shindo and Matsumoto (2016) and Plutchik (2001a) presented how the emotions can be mixed. Using the concepts of *family of emotions* is possible to define a set of *family of mixed emotions*. Table 2 lists emotion family combinations two by two, and the family mixed emotions obtained.

According to Table 2, F_{love} is the mix of F_{joy} and F_{trust}. Here, is proposed to use vector sum to mix emotions. Let $\vec{v}_x = \alpha_x \vec{e}_x, \vec{v}_x \in F_{\text{joy}}$, and $\vec{v}_y = \alpha_y \vec{e}_y, \vec{v}_y \in F_{\text{trust}}$. Therefore,

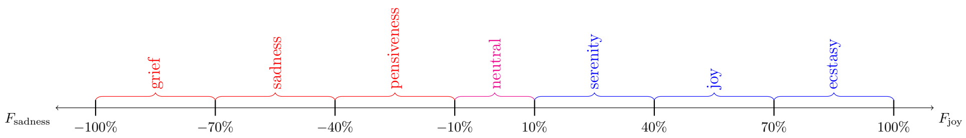

Figure 24 – Graphical representation of the x axis using mapToLevels $(\vec{v})$ mapping

Source – By author.

Table 2 – Families emotions combinations

basic families emotions	mixed family emotion	basic families emotions	mixed familiy emotion
$F_{\text{joy}}, F_{\text{trust}}$	F_{love}	$F_{\text{sadness}}, F_{\text{disgust}}$	F_{remorse}
$F_{\text{joy}}, F_{\text{fear}}$	F_{guilt}	$F_{\text{sadness}}, F_{\text{anger}}$	envy
$F_{\text{joy}}, F_{\text{surprise}}$	F_{delight}	$F_{\text{sadness}}, F_{\text{anticipation}}$	$F_{\text{pessimism}}$
$F_{\text{trust}}, F_{\text{fear}}$	$F_{\text{submission}}$	$F_{\text{disgust}}, F_{\text{anger}}$	F_{contempt}
$F_{\text{trust}}, F_{\text{surprise}}$	$F_{\text{curiosity}}$	$F_{\text{disgust}}, F_{\text{anticipation}}$	F_{cynicism}
$F_{\text{trust}}, F_{\text{sadness}}$	$F_{\text{sentimentality}}$	$F_{\text{disgust}}, F_{\text{joy}}$	$F_{\text{morbidness}}$
$F_{\text{fear}}, F_{\text{surprise}}$	F_{awe}	$F_{\text{anger}}, F_{\text{anticipation}}$	$F_{\text{aggression}}$
$F_{\text{fear}}, F_{\text{sadness}}$	F_{despair}	$F_{\text{anger}}, F_{\text{joy}}$	F_{pride}
$F_{\text{fear}}, F_{\text{disgust}}$	F_{shame}	$F_{\text{anger}}, F_{\text{trust}}$	$F_{\text{dominance}}$
$F_{\text{surprise}}, F_{\text{sadness}}$	$F_{\text{disappointment}}$	$F_{\text{anticipation}}, F_{\text{joy}}$	F_{optimism}
$F_{\text{surprise}}, F_{\text{disgust}}$	F_{unbelief}	$F_{\text{anticipation}}, F_{\text{trust}}$	F_{hope}
$F_{\text{surprise}}, F_{\text{anger}}$	F_{outrage}	$F_{\text{anticipation}}, F_{\text{fear}}$	F_{anxiety}

Source – Adapted from (PLUTCHIK, 2001a)

$\vec{v}_{xy} \in F_{\text{love}}$ is obtained using:

$$\begin{aligned}
\vec{v}_{xy} &= \vec{v}_x + \vec{v}_y \\
&= \alpha_x \vec{e}_x + \alpha_y \vec{e}_y \\
&= \alpha_x \begin{bmatrix} 1 & 0 & 0 & 0 \end{bmatrix}^{\mathtt{T}} + \alpha_y \begin{bmatrix} 0 & 1 & 0 & 0 \end{bmatrix}^{\mathtt{T}} \\
&= \begin{bmatrix} \alpha_x & \alpha_y & 0 & 0 \end{bmatrix}^{\mathtt{T}}.
\end{aligned}$$

To represent dyads (primary, secondary, and tertiary) proposed by Plutchik (2001a), it is necessary that two out of the four parameters $(\alpha_x, \alpha_y, \alpha_z, \alpha_w)$ are equals to zero (RODRIGUES; ASLA; VELHO, 2009).

3.3 ROS IMPLEMENTATION

ROS was presented in Chapter 2 as a tool that allows development of all parts of the robot system in a modular way. In this work the system was divided in ROS nodes that are responsible for the tasks of: `control_law`, used to specify the control law the robot uses to follow the child; `child_detection`, to process laser scan data and identify if a child was detect and his/her position; `workspace`, to define specific spaces where the robot can move; `state_machine`, to execute a state machine in which the robot brings near or distances itself of the child; `emotion_detection`, to determine robot emotion;

RosMARIA, a ROS interface to access data from odometry of and to operate the robot MARIA-T21; marialog, to save all data in a log file.

Considering that the robot MARIA-T21 is in development in parallel to this work, and in order to allow the development of the controllers independently to the availability of the robot a RosAria node was used, that is a ROS interface to access Aria Sofware that allows controlling a Pioneer Robot in real or simulated environment.

In the same way, considering the pandemic and the difficult to make experiments with a child, in this work a testkid ROS node was used that simulates a laser scan reading a path realized by a child.

Figure 25 shows all ROS nodes and their relationships. Next sections will detail all nodes and their applications, with a special attention in Section 3.3.7 to the node responsible for control law.

3.3.1 Laser emulation

Node testekid implements a simulation of a child position and his/her movements throughout the space. It simulates a laser distance sensor too, which detects the child and publishes him/her position. To do that, this node uses a robot position that can be provided by the odometry of the robot or in simulation by the RosAria node, because distance sensor LiDAR is localized on top of the robot and its center is concentric with robot center. The pose topic has ROS nav_msgs/Odometry messages with position and orientation data, that can be used to determine a pose information (see Figure 26 to details of message's structure). This pose can be represented as a vector $\vec{\xi}_R = \begin{bmatrix} x_R & y_R & \psi \end{bmatrix}^\mathtt{T}$. The child position is defined according to a specific path, simulating movement of a child in an interaction with the robot. Each position can be represented as a vector $\vec{\xi}_K = \begin{bmatrix} x_K & y_K & \gamma \end{bmatrix}^\mathtt{T}$ where (x_K, y_K) is the point of space where child is, and $\gamma = \arctan \frac{y_K - y_R}{x_K - x_R}$ is the angle between the child's front and X^W axis.

Therefore, it is possible to calculate distance (ρ) and angle (α) between the robot and the child using Equation 3.5:

$$\begin{aligned} \rho &= \sqrt{(x_K - x_R)^2 + (y_K - y_R)^2} \\ \alpha &= \gamma - \psi. \end{aligned} \tag{3.5}$$

Distance and angle are published using a ROS sensor_msgs/LaserScan message in testekid/laserscan topic[2]. This message permits only integer values for angles. So, always there will be an error of rounding (maximum error will be of $0.5° \approx 8.7 \times 10^{-3}$ rad). For example, if $\alpha = 0.25°$, it will be published as $\alpha = 0°$, otherwise, if $\alpha = 0.51°$, it will be

[2] see <http://docs.ros.org/en/melodic/api/sensor_msgs/html/msg/LaserScan.html> to details of message's structure

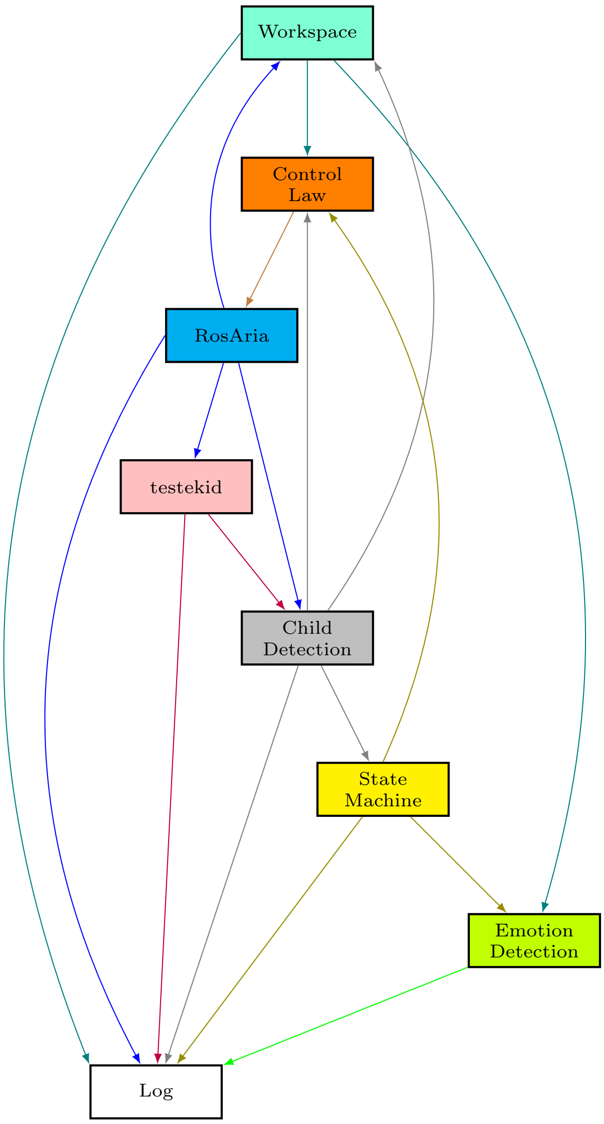

Figure 25 – ROS Nodes' Relationship

Source – By author.

published as $\alpha = 1°$. To test how this rounding impacts in measurements, two tests were conducted, with the robot stopped in the origin of global axis: a measurement of a circle with radius $r = 1\,\text{m}$, and a measurement of a square with a side $l = 1\,\text{m}$.

This node publishes the child position simulated at time, using a custom message called `Position` in the `testekid/position` topic (see Code A.1 to details of message's structure).

When the tests are performed with children, the part of laser simulation will be changed for a real laser distance sensor creating a node to get laser data and to publish values obtained using ROS `sensor_msgs/LaserScan` message.

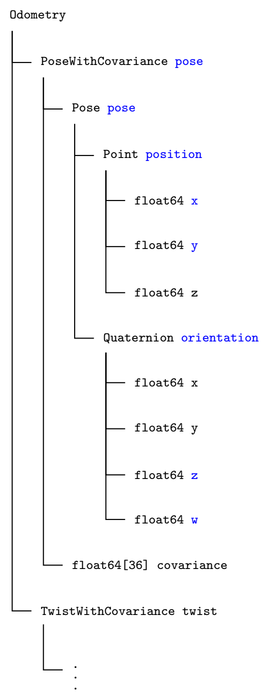

Figure 26 – Odometry message's structure with fields used by `testekid` highlighted in blue

Source – By author.

3.3.2 Child Detection

This node receives position data from `RosAria` node identifying where the robot is in *Work Area* and laser sensor data from `testekid` node with distances and angles that were measured.

Messages from `sensor_msgs/LaserScan` have a range of 360 distances (corresponding to a distance in each degree). The node finds minor distance and angle of this distance. Then, it publishes a message about if a child is detected and where he/she is localized (see Code A.2 to details of message's structure). It is made considering that the child is the nearest point to the robot in all directions.

3.3.3 Workspace

To observe *Workspace* defined in Section 3.1, the `workspace` node was created. It receives robot position data from `RosAria` (or `RosMARIA`) node and child position from `child_detection` node. Using these data, this node can identify if child is in *external area*, *internal area*, or *observation area*, publishing a message containing this data (see Code A.3 to details of message's structure).

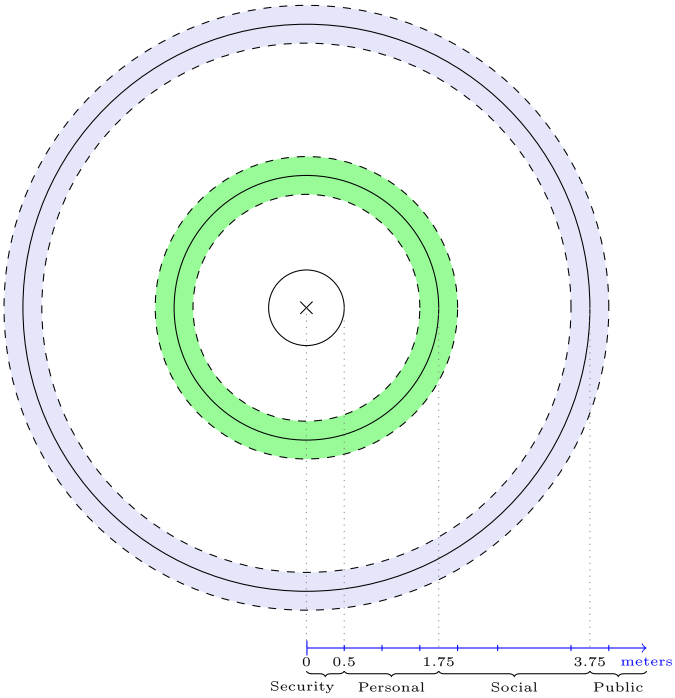

Figure 27 – Graphical representation of proxemic zones

Source – By author.

3.3.4 State Machine

According to proxemics zones presented in Section 2.2.1 this work selects to use concentric circles, parallel to the floor, that are defined around the robot. First area A_1, that represents *security area*, is a circle, whose center coincides with the center of the robot and the diameter is $\phi_{A_1} = 0.5\,\mathrm{m}$. Second area A_2, that represents *personal area*, is an annulus, concentric with A_1, whose outer circle has diameter $\phi_{A_2}^{\mathrm{out}} = 1.75\,\mathrm{m}$ and inner circle has diameter $\phi_{A_2}^{\mathrm{inn}} = 0.5\,\mathrm{m}$. Third area A_3, that represents *social area*, is an annulus, concentric with A_1, whose outer circle has diameter $\phi_{A_3}^{\mathrm{out}} = 3.75\,\mathrm{m}$ and inner circle has diameter $\phi_{A_3}^{\mathrm{inn}} = 1.75\,\mathrm{m}$. And the fourth area A_4, that represents *public area*, is the area outside of the circle with diameter $\phi_{A_4} = 3.75\,\mathrm{m}$. Figure 27 shows these areas.

Two auxiliary proxemic zones are defined: *social/public* and *personal/social*; these zones are annulus, concentrics with A_1, and are used in the control law associated with a specific state machine to provide the robot with a soft movement of approximation. They are visualized as colored annulus in Figure 27: lavender to *social/public*, with $\phi_{A_L}^{\mathrm{in}} = 1.5\,\mathrm{m}$ and $\phi_{A_L}^{\mathrm{out}} = 2\,\mathrm{m}$; and pale-green to *personal/social*, with $\phi_{A_G}^{\mathrm{in}} = 3.5\,\mathrm{m}$ and $\phi_{A_G}^{\mathrm{out}} = 4\,\mathrm{m}$.

Figure 28 presents the state machine implemented in `state_machine` node and used in this work, where d is the distance that will be reduced to d_i (given in meters), d_i is the desired distance (also given in meters), and Δt is the time it takes to confirm a change of state. Each rounded rectangle represents a *proxemic zone*.

In the beginning, $\mathrm{prox}(d) = \mathrm{public}$, meaning the robot is on a *public zone*, and the

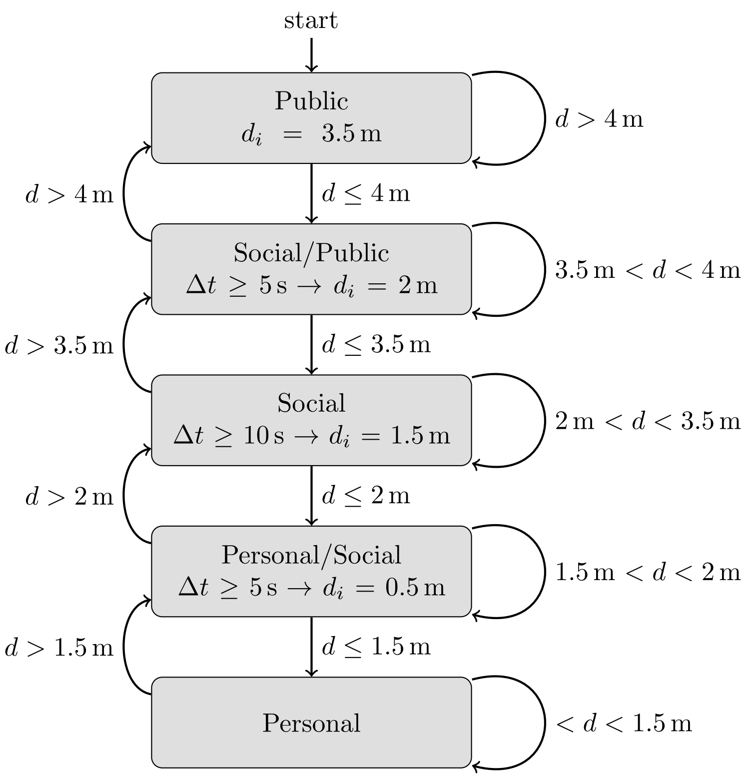

Figure 28 – State machine used in this work to implement the concepts of *proxemic zones*

Source – Piero, Caldeira and Bastos Filho (2020).

desired distance, d_i, is set to 3.5 m, with the intention of going to the *social/public zone*.

To ensure an approach that gives the child the opportunity to distance himself/herself, the robot uses the auxiliary *social/public zone* where the robot stays waiting for 5 s to confirm if the child accepts its proximity. If the child does not run away from the robot, it represents a confirmation of the acceptance. So the robot modifies the desired distance ($d_i = 2\,\mathrm{m}$) to reach the *social zone*. Otherwise, if the child distances himself/herself, then the logic of the state machine sets $\mathrm{prox}(d) = \mathrm{public}$. The same logic is employed in others *proxemic zones*, with different times and desired distances, which can be seen in Figure 28.

This node publishes two different types of messages: one for each *proxemic zone*'s change (see Code A.4 to details of message's structure); and another containing the desired distance (see Code A.5 to details of message's structure).

3.3.5 Demonstrating emotions

To calculate the robot emotion, the node `emotion_detection` uses data from *State Machine* (see Section 3.3.4) and proximity between robot and border of *internal area* published by `workspace` node.

When the state of *State Machine* changes from *Social/Public* to *Public*, the node identifies that child is going far away and, therefore, the robot expresses *grief*. But if

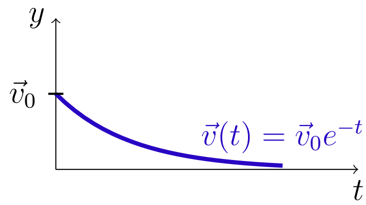

Figure 29 – Decay function

Source – By author.

the state changes from *Social/Public* to *Social*, the node identifies that child is accepting contact and the robot expresses *happiness*.

On the other hand, if the state changes from *Personal/Social* to *Social* the node identifies the child's intention to move away and expresses *sadness*. While, if the state changes from *Personal/Social* to *Personal* then node identifies a greater interest in proximity between the robot and the child and, therefore, the robot express *ecstasy*.

Using proximity between robot and border of *internal area* this node can express *fear*.

To express these emotions this node uses *Emotion Hypercube* vector $\vec{v}_e$ (see Section 3.2). So, *grief* is represented using $\vec{v}_{\text{grief}} = \begin{bmatrix}-100 & 0 & 0 & 0\end{bmatrix}^{\mathsf{T}}$, *happiness* using $\vec{v}_{\text{happiness}} = \begin{bmatrix}50 & 0 & 0 & 0\end{bmatrix}^{\mathsf{T}}$, *sadness* using $\vec{v}_{\text{sadness}} = \begin{bmatrix}-50 & 0 & 0 & 0\end{bmatrix}^{\mathsf{T}}$, and *ecstasy* using $\vec{v}_{\text{ecstasy}} = \begin{bmatrix}100 & 0 & 0 & 0\end{bmatrix}^{\mathsf{T}}$. To represent *fear* was used $\vec{v}_{\text{fear}} = \begin{bmatrix}0 & 0 & \alpha_z & 0\end{bmatrix}^{\mathsf{T}}$, where α_z is proportional to proximity between robot and border of *internal area*.

Nevertheless, these emotions are not constants and vary from start value to 0 using a decay function defined according to Equation 3.6 (Figure 29 shows function's graph):

$$\vec{v}(t) = \vec{v}_0 e^{-t}, \tag{3.6}$$

where $\vec{v}_0$ is the initial value, and $\vec{v}(t) \to 0$ in up to 5 seconds (because decay constant $\tau = 1$).

This node publishes an emotion detection message (see Code A.6 to details of message's structure).

3.3.6 RosAria

To access robot platform or to simulate a robot in computer is used `RosAria`[3] node that provides a ROS interface for some robots like Pioneer 3DX (HEDGES, 2018) used in first and second MARIA's versions. This interface permits the control of linear and angular velocities through `twist` message (see Figure 30 for more details).

[3] <http://wiki.ros.org/ROSARIA>

```
Twist
├── Vector3 linear
│   ├── float64 x
│   ├── float64 y
│   └── float64 z
└── Vector3 angular
    ├── float64 x
    ├── float64 y
    └── float64 z
```

Figure 30 – Twist message's structure, with fields used by `RosAria` highlighted in blue

Source – By author.

When the new prototype `MARIA-T21` is finished, `RosAria` node will be replaced by `RosMARIA` node which will use the `twist` message to receive linear and angular velocities.

3.3.7 Control Law

This is the main node that is responsible for robot control, determining how the robot moves to execute *State Machine* proposed in Section 3.3.4.

The robotic platform used in MARIA and N-MARIA, and simulated on MobileSim [4], is an Omron Adept MobileRobots Pioneer 3-DX. This robotic platform is a differential drive (unicycle-like) robot, with two motorized wheels, and one free wheel. Instead of controlling the right speed and the left speed of the drive systems, the unicycle-like model uses v (linear velocity) and ω (angular velocity) as control parameters, as the robotic platform has a low-level controller that converts these velocities in commands for each motor.

The control law adopted in this work (adapted from a control law proposed by (CARELLI, 2018)) to move the robot from a current position to a goal position (according to as shown in Figure 31) is:

$$
\begin{aligned}
\xi &= \frac{1}{1+\exp(100\dot{\rho})} \\
v &= K_v \xi \rho \cos\alpha \\
\omega &= K_r (K_\omega \tanh\alpha + v\frac{\sin\alpha}{\rho})
\end{aligned}
\tag{3.7}
$$

where:

v is the linear velocity sent to robot [m/s];

[4] MobileSim disponible at https://github.com/srmq/MobileSim

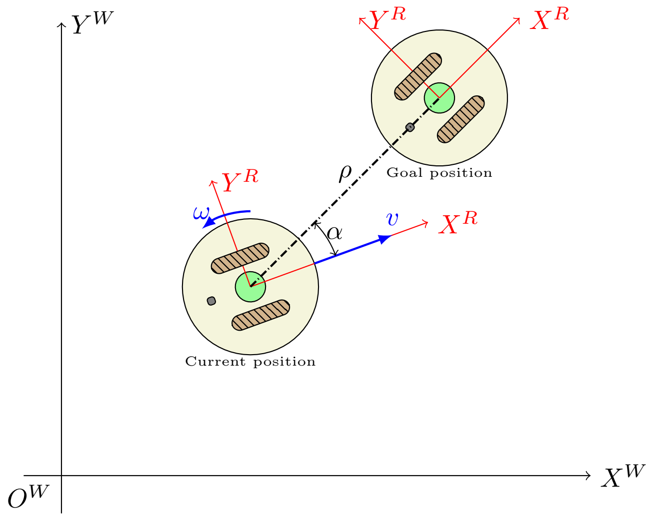

Figure 31 – Objective of movement

Source – By author.

ω is the angular velocity sent to robot [rad/s];

ρ is the linear distance between where the robot is and the desired position [m];

ξ is the *Walk-off Factor*, which ensures that the child can move away without the robot following him/her;

α is the angular difference between where the robot's front is and the desired head angle [rad];

$K_v = 0.1\,\mathrm{s}^{-1}$, $K_\omega = 1\,\mathrm{s}^{-1}$ are empirically determined gains;

$K_r = 0.5\,\mathrm{rad}$ is a constant to adjust units of measurement.

To show controller's stability, the Equation 2.2, initially presented in Section 2.3, is reviewed:

$$\dot{\rho} = -v\cos\psi$$
$$\dot{\psi} = -\omega + \frac{v\sin\psi}{\rho}.$$

Figure 31 helps to remember each data used in this equation.

Taking $\begin{bmatrix}\rho\\ \alpha\end{bmatrix} = \begin{bmatrix}0\\ 0\end{bmatrix}$ as a point of equilibrium, and considering

$$V(\rho,\alpha) = \frac{\rho^2}{2} + \frac{\alpha^2}{2} \tag{3.8}$$

as a Lyapunov candidate function (SILVA, 2006), the first time derivative is given by

$$
\begin{aligned}
\dot{V}(\rho,\alpha) &= \rho\dot{\rho} + \alpha\dot{\alpha} \\
&= \rho(-v\cos\alpha) + \alpha\left(-\omega + \frac{v\sin\alpha}{\rho}\right) \\
&= \rho\left(-\underbrace{(K_v\xi\rho\cos\alpha)}_{v}\cos\alpha\right) + \alpha\left(\underbrace{-\cancelto{1}{K_r}\left(K_\omega\tanh\alpha + v\frac{\cancel{\sin\alpha}}{\cancel{\rho}}\right)}_{\omega} + \cancel{\frac{v\sin\alpha}{\rho}}\right) \\
&= -K_v\xi(\rho\cos\alpha)^2 - K_\omega\alpha\tanh\alpha \\
&\leq 0
\end{aligned}
\tag{3.9}
$$

which is negative semi definite, and therefore $V(\rho,\alpha)$ is a Lyapunov function.

$\dot{V}(\rho,\alpha)$ can be shown that is negative definite using :

$$
\begin{aligned}
f_1(\rho,\alpha) &= -K_v\xi(\rho\cos\alpha)^2 \\
f_1(\rho,\alpha) &= 0 \iff \rho = 0 \text{ and/or } \alpha = \pi \\
\\
f_2(\rho,\alpha) &= -K_\omega\alpha\tanh\alpha \\
f_2(\rho,\alpha) &= 0 \iff \alpha = 0, \forall\rho \\
\\
\dot{V}(\rho,\alpha) &= f_1(\rho,\alpha) + f_2(\rho,\alpha) \\
\dot{V}(\rho,\alpha) &= 0 \iff \rho = 0 \text{ and } \alpha = 0.
\end{aligned}
$$

Hence, because $V(\rho,\alpha)$ is a Lyapunov function and $\dot{V}(\rho,\alpha)$ is negative definite then the system, when controlled through this control law, has an asymptotically stable equilibrium at the origin, which means that $\rho \to 0$ and $\alpha \to 0$ as $t \to \infty$.

This chapter demonstrates how the emotion is calculated and is made available. It also shows how ROS is used to create nodes responsibles for executing control law, determining where the robot is and where the child is and how the interaction between the robot and the child will occur.

The next chapter will present the results obtained and some discussions about them.

4 RESULTS AND DISCUSSION

[...] Take heart and be strong; have no fear and do not be troubled; for the Lord your God is with you wherever you go.

Joshua, 1, 9

In this chapter, simulations of the interaction between the robot and a child are presented. Its results are analyzed and a discussion is made about implementation.

4.1 EXPERIMENTS

First, it is shown how the control law works. To do that, the robot starts the simulations on $(0,0)$ in global axis $\langle O^W, X^W, Y^W \rangle$. Five points to reach were proposed: $A = (2,0), B = (0,2), C = (-2,0)$, and $D = (0,-2)$.

In Figure 32 is shown robot's data for displacement from $O^W = (0,0)$ to $A = (2,0)$. The maximum linear velocity reached is of 0.2 m/s and there was not angular velocity. There is a noise of 1.46 % in goal position, specifically in x dimension, that is resulting from sensor distance's displacement (because the sensor moves together with the robot).

Figure 33 shows robot's data for displacement from $O^W = (0,0)$ to $B = (0,2)$. In this case, linear velocity reaches 0.17 m/s and angular velocity reaches 0.45 rad/s. Again, there is a error in goal position (in x and in y positions) of 0.91 %. This noise impacts mainly in angular velocity and in head's angle, because they are more susceptible to distances variations.

Robot's data for displacement from $O^W = (0,0)$ to $C = (-2,0)$ is shown in Figure 34. In this case, first the robot moves backward and then goes to reach C, so the linear velocity varies from 0 to -0.20 m/s and then to 0.14 m/s. The angular velocity reaches 0.51 rad/s. Anew, here is a noise in goal position (in x and in y positions) of 1 %; impacting mainly in angular velocity and in head's angle.

In Figure 35, which contains robot's data for displacement from $O^W = (0,0)$ to $D = (0,-2)$, is shown that linear velocity reaches 0.17 m/s and angular velocity reaches -0.45 rad/s. The present error is of 1 % and affects angular velocity and head's angle.

In four experiments, the average displacement velocity is of 0.3 m/s. This allows the child to run away if he/she feels fear, for example, because a child can move at least 0.6 m/s (MOREIRA et al., 2006; FRANCO, 2009).

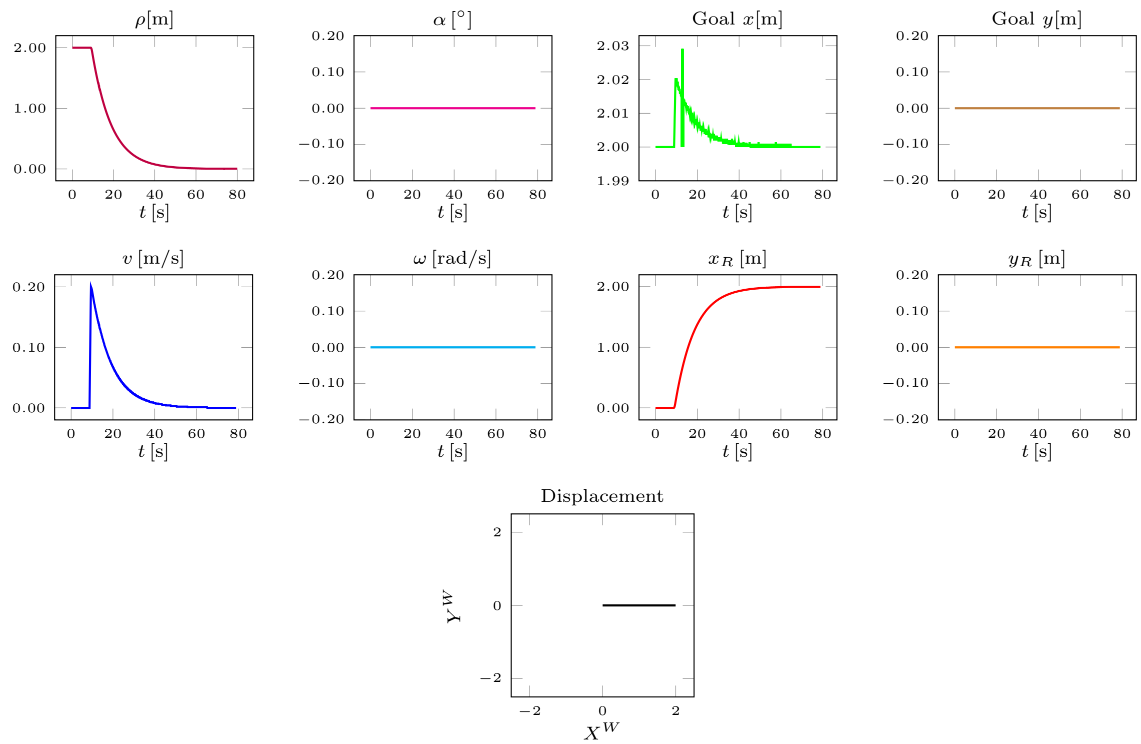

Figure 32 – Robot's data for displacement from $O^W = (0, 0)$ to $A = (2, 0)$

Source – By author.

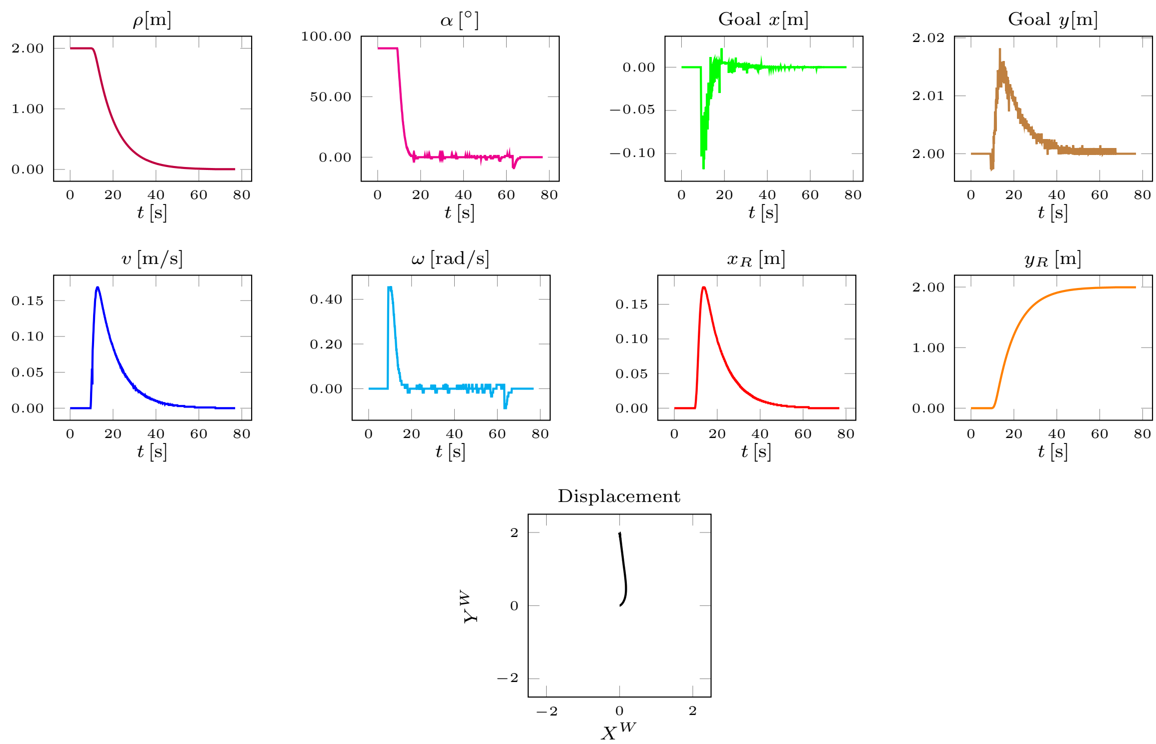

Figure 33 – Robot's data for displacement from $O^W = (0, 0)$ to $B = (0, 2)$

Source – By author.

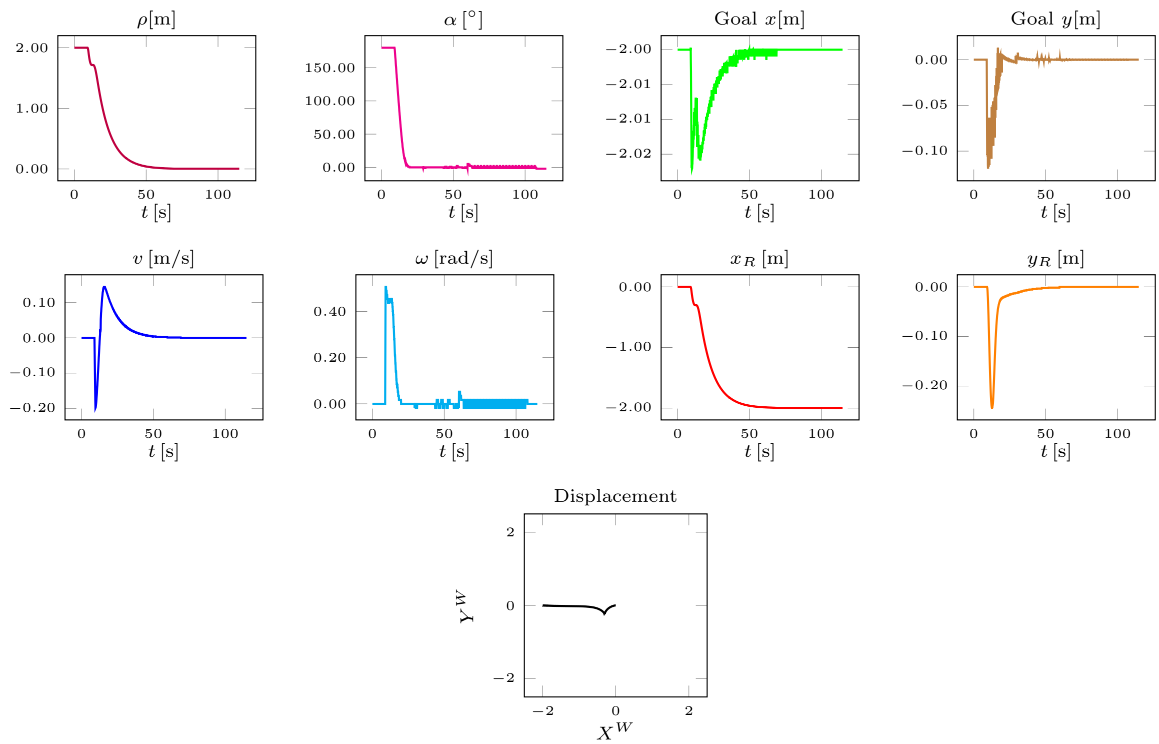

Figure 34 – Robot's data for displacement from $O^W = (0, 0)$ to $C = (-2, 0)$

Source – By author.

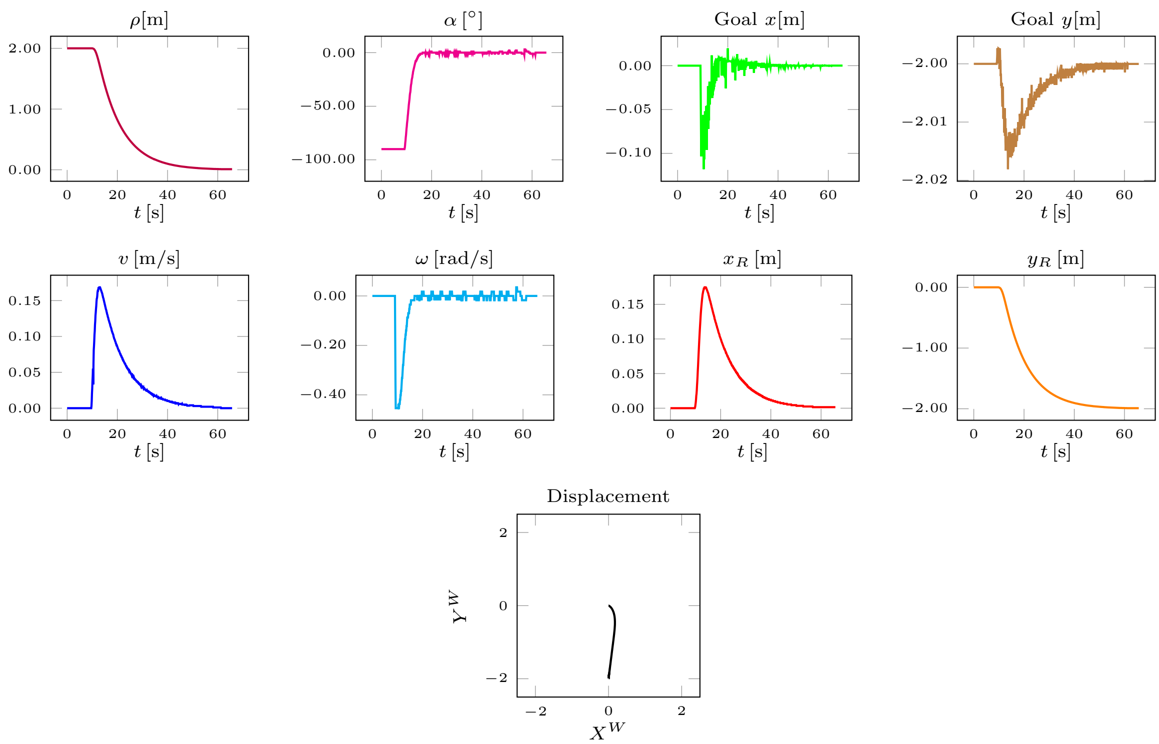

Figure 35 – Robot's data for displacement from $O^W = (0, 0)$ to $D = (0, -2)$

Source – By author.

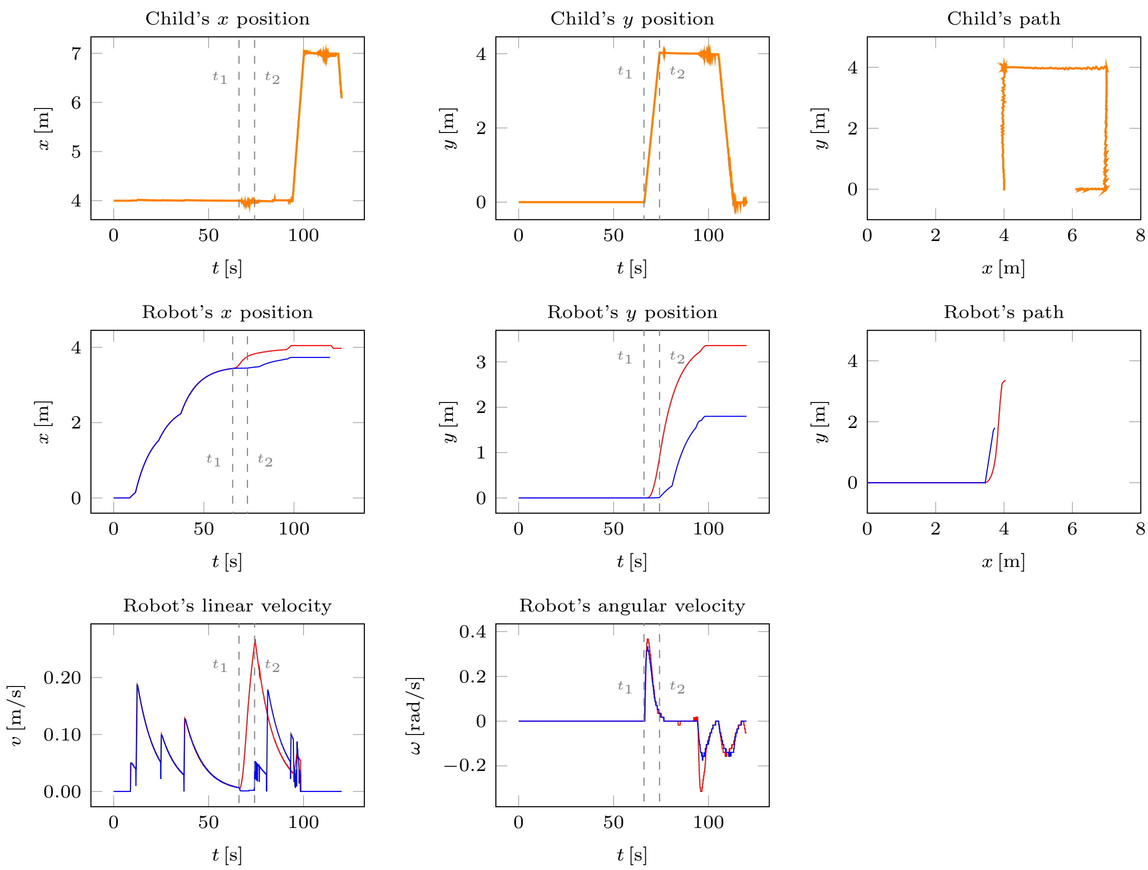

Figure 36 – Comparison between controller with (in blue) and without (in red) *Walk-off factor*

Source – By author.

4.1.1 Walk-off factor

To show how the *Walk-off factor* impacts the controller, a simulation was proposed where the child starts in interaction area accepting the approach of the robot, then he/she demonstrates fear and walks off. Figure 36 shows the child's path in orange and the robot's controller data in blue (when the *Walk-off factor* is used) and red (when the *Walk-off factor* is not used). Until $t_1 = 66\,\mathrm{s}$, the child stays still in $(4, 0)$, in global axis, and the robot moves to approach to the child, then at $t_1 = 66\,\mathrm{s}$ the child goes away moving to $(4, 4)$, that is reached at $t_2 = 74.2\,\mathrm{s}$; when the *Walk-off factor* is not used, the robot follows the child, on the other hand, when the *Walk-off factor* is used the robot respects child's will and does not move. This can be visualized in Figure 36 when the robot's linear velocity goes to and stays in zero between t_1 and t_2. The presence or the absence of this factor impacts in robot's displacements, which can also be visualized in Figure 36.

4.1.2 Simulations

To simulate possible interactions between a child and the robot, first it is necessary to define how a child path is implemented.

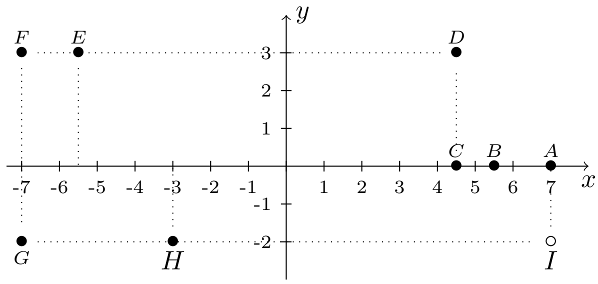

Figure 37 – An example of a *Path*

Source – Piero, Caldeira and Bastos Filho (2020)

A *PointPath* is defined as a vector with four elements: a pair (x, y) representing localization of the child in global reference $\langle O^W, X^W, Y^W\rangle$, a quantity of seconds, Δt, which is spent at this position, and a direction to displacement for the next *PointPath*, $\Delta s \in \{\text{left } (\leftarrow), \text{ right } (\rightarrow), \text{ up}(\uparrow), \text{ or down } (\downarrow)\}$. Therefore, a *PointPath* is represented as $P_P = \begin{bmatrix} x & y & \Delta t & \Delta s \end{bmatrix}^\intercal$.

A *Path* is defined as an ordered list of *PointPath*, where the first represents the begin and the end of the Path. All paths are, necessarily, closed circuits and continuous, so, for simulations, the child starts the path on beginner *PointPath*, then crosses all elements of *Path* in sequence until reaches the last *PointPath*, and, finally, goes to the first again and repeats. A velocity of 0.5 m/s is maintained between consecutive points. The *Path* is used in node `testekid` to create a simulation of child's displacement.

Figure 37 shows an example of a *Path* P where the simulation starts on point A. This example can be defined as:

$$P = \left\{ \underbrace{\begin{bmatrix} 7 \\ 0 \\ 7 \\ \leftarrow \end{bmatrix}}_{A}, \underbrace{\begin{bmatrix} 5.5 \\ 0 \\ 5 \\ \leftarrow \end{bmatrix}}_{B}, \underbrace{\begin{bmatrix} 4.5 \\ 0 \\ 20 \\ \uparrow \end{bmatrix}}_{C}, \underbrace{\begin{bmatrix} 4.5 \\ 3 \\ 25 \\ \leftarrow \end{bmatrix}}_{D}, \underbrace{\begin{bmatrix} -5.5 \\ 3 \\ 15 \\ \leftarrow \end{bmatrix}}_{E}, \underbrace{\begin{bmatrix} -7 \\ 3 \\ 2 \\ \downarrow \end{bmatrix}}_{F}, \underbrace{\begin{bmatrix} -7 \\ -2 \\ 2 \\ \rightarrow \end{bmatrix}}_{G}, \underbrace{\begin{bmatrix} -3 \\ -2 \\ 30 \\ \rightarrow \end{bmatrix}}_{H}, \underbrace{\begin{bmatrix} 7 \\ -2 \\ 2 \\ \uparrow \end{bmatrix}}_{I} \right\}$$

Two simulated paths, which were empirically determined, were proposed: P_1 and P_2, defined as:

- $$P_1 = \left\{ \underbrace{\begin{bmatrix} 7 \\ 0 \\ 5 \\ \leftarrow \end{bmatrix}}_{A}, \underbrace{\begin{bmatrix} 5.5 \\ 0 \\ 5 \\ \leftarrow \end{bmatrix}}_{B}, \underbrace{\begin{bmatrix} 4.5 \\ 0 \\ 10 \\ \uparrow \end{bmatrix}}_{C}, \underbrace{\begin{bmatrix} 4.5 \\ 3 \\ 10 \\ \leftarrow \end{bmatrix}}_{D}, \underbrace{\begin{bmatrix} -5.5 \\ 3 \\ 10 \\ \leftarrow \end{bmatrix}}_{E}, \underbrace{\begin{bmatrix} -7 \\ 3 \\ 10 \\ \downarrow \end{bmatrix}}_{F}, \underbrace{\begin{bmatrix} -7 \\ -2 \\ 10 \\ \rightarrow \end{bmatrix}}_{G}, \underbrace{\begin{bmatrix} -3 \\ -2 \\ 10 \\ \rightarrow \end{bmatrix}}_{H}, \underbrace{\begin{bmatrix} 7 \\ -2 \\ 10 \\ \uparrow \end{bmatrix}}_{I} \right\}$$

- $P_2 = \left\{ \underbrace{\begin{bmatrix} 7 \\ 0 \\ 5 \\ \leftarrow \end{bmatrix}}_{A}, \underbrace{\begin{bmatrix} 4 \\ 0 \\ 30 \\ \rightarrow \end{bmatrix}}_{B}, \underbrace{\begin{bmatrix} 5.5 \\ 0 \\ 30 \\ \uparrow \end{bmatrix}}_{C}, \underbrace{\begin{bmatrix} 5.5 \\ 4.5 \\ 30 \\ \leftarrow \end{bmatrix}}_{D}, \underbrace{\begin{bmatrix} -5.5 \\ 4.5 \\ 30 \\ \downarrow \end{bmatrix}}_{E}, \underbrace{\begin{bmatrix} -5.5 \\ -4.5 \\ 30 \\ \rightarrow \end{bmatrix}}_{F}, \underbrace{\begin{bmatrix} 7 \\ -4.5 \\ 30 \\ \uparrow \end{bmatrix}}_{G} \right\}$

Another definition that was made is about *Workspace*, which is presented in Section 3.1. Remembering, there are four parameters that delimits special areas, *internal* (where there are interaction between the robot and the child), *observation* (where the child can be when feeling fear, for example), and *external* (where there are not actions by the robot): $X_{\text{int}}, X_{\text{ext}}, Y_{\text{int}}$, and Y_{ext}. For simulations the following values were proposed (Figure 38 shows the *Workspace* obtained, with the robot in its initial pose):

- $X_{\text{int}} = 5\,\text{m}$, $Y_{\text{int}} = 4\,\text{m}$;
- $X_{\text{ext}} = 6\,\text{m}$, $Y_{\text{ext}} = 5\,\text{m}$,

4.1.3 Analysis of first *Path*

In this section the Path P_1 is analyzed (graphically represented in Figure 39). To facilitate analysis, the Path is divided into nine steps: $P_A \rightarrow P_B$, $P_B \rightarrow P_C$, …, $P_H \rightarrow P_I$, and $P_I \rightarrow P_A$.

The simulation starts and spends 5.7 s to configure all ROS nodes (and according to what is proposed in *State Machine*, the desired distance is set to $d_i = 3.5\,\text{m}$), then, at $t_1 = 5.7\,\text{s}$, the child starts the simulation in *external area*, on $P_A = \begin{bmatrix} 7 & 0 & 5 & \leftarrow \end{bmatrix}^{\mathtt{T}}$, waits for 5 s and then, at $t_2 = 10.7\,\text{s}$, starts traveling to reach P_B. While the child was on P_A there were no actions executed by the robot, which is in accordance with what has been proposed. At $t = 12.8\,\text{s}$ the `Workspace` node detects that the child enters in *observation area*, then the `Control Law` starts to send velocities commands. The child reaches $P_B = \begin{bmatrix} 5.5 & 0 & 5 & \leftarrow \end{bmatrix}^{\mathtt{T}}$ at $t_3 = 13.7\,\text{s}$, stops and then waits for 5 s. Figure 40 shows robot's data during the displacement of child from P_A to P_B.

In second step, at $t_4 = 18.7\,\text{s}$, the child exits from P_B and travels to reach P_C. He/she spends 2 s and at $t_5 = 20.7\,\text{s}$ reaches P_C entering in *internal area*. There, he/she waits for 10 s and finally, at $t_6 = 30.7\,\text{s}$, starts the next movements trying to reach P_D. While the child approaches, the robot keeps the distance stipulated by proxemics ($d_i = 3.5\,\text{m}$) and travels to back (inputting a negative linear velocity). Figure 41 shows robot's data during the displacement of child from P_B to P_C.

Third, the child goes from P_C to reach P_D. This is to simulating that the child observes the robot and intends to keep distance (because surprise, for example). After

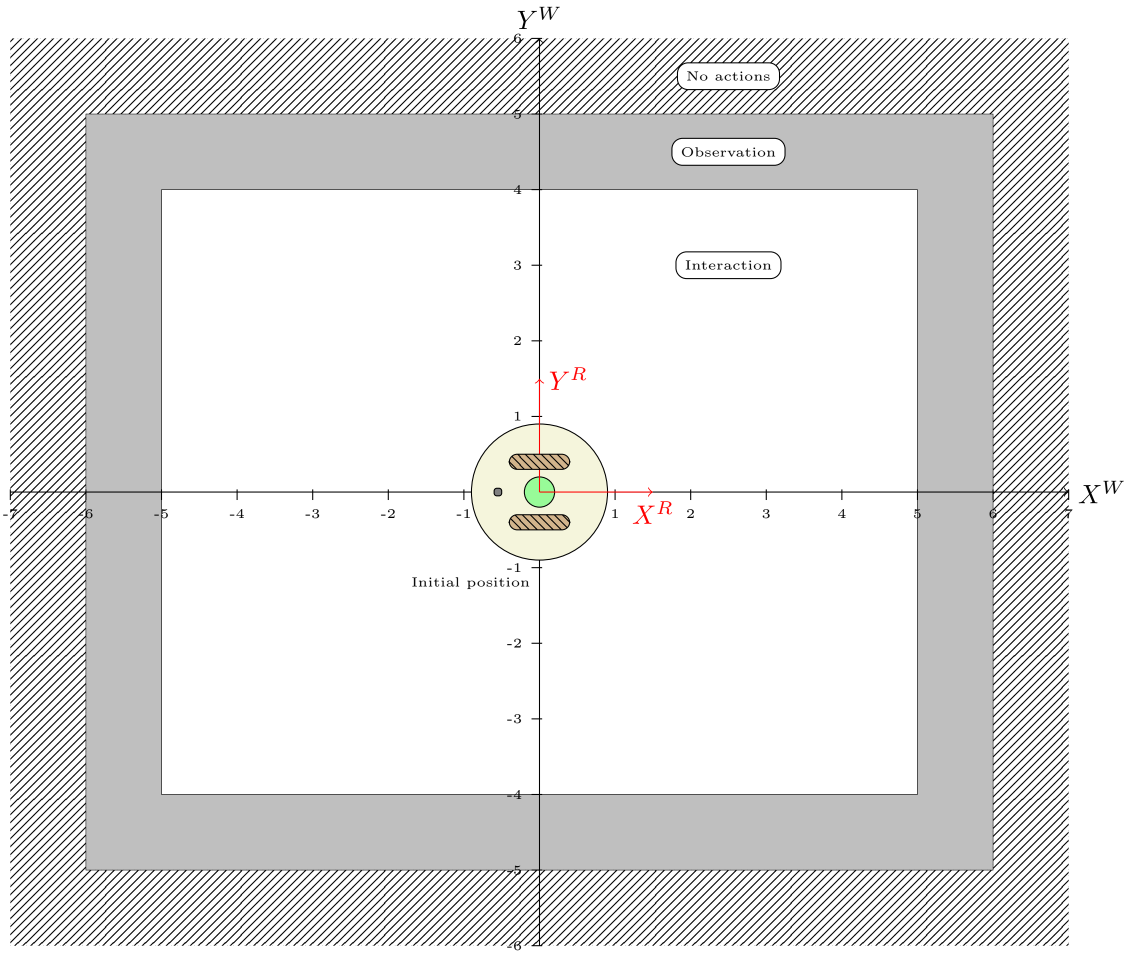

Figure 38 – Workspace proposed for simulations

Source – By author.

$t_6 = 30.7\,\text{s}$, when the child goes away increasing distance from the robot, it is observed that the robot respects child's intention and does not follows him/her, due to the *Walk Off's Factor*. The child stopped at $t_7 = 36.7$ in interaction area and waited for robot's approximation. Figure 42 shows robot's data during the displacement of child from P_C to P_D.

In the fourth step, the child goes from P_D to reach P_E, simulating a desire to go to *observation area*. At $t_8 = 46.7\,\text{s}$ the child starts the movements to reach P_E, what happened at $t_0 = 66.7\,\text{s}$. After t_9 the `workspace` node detects the observation distance which influences the control law. Figure 43 shows robot's data during the displacement of child from P_D to P_E.

Figures 44, 45, 46, 47, and 48 show robot's data during the displacement of child from P_E to P_F, P_F to P_G, P_G to P_H, P_H to P_I, and P_I to P_A, respectively. It is possible to observe that every moment that child distances herself/himself from the robot, the robot identifies this intention and does not follow the child.

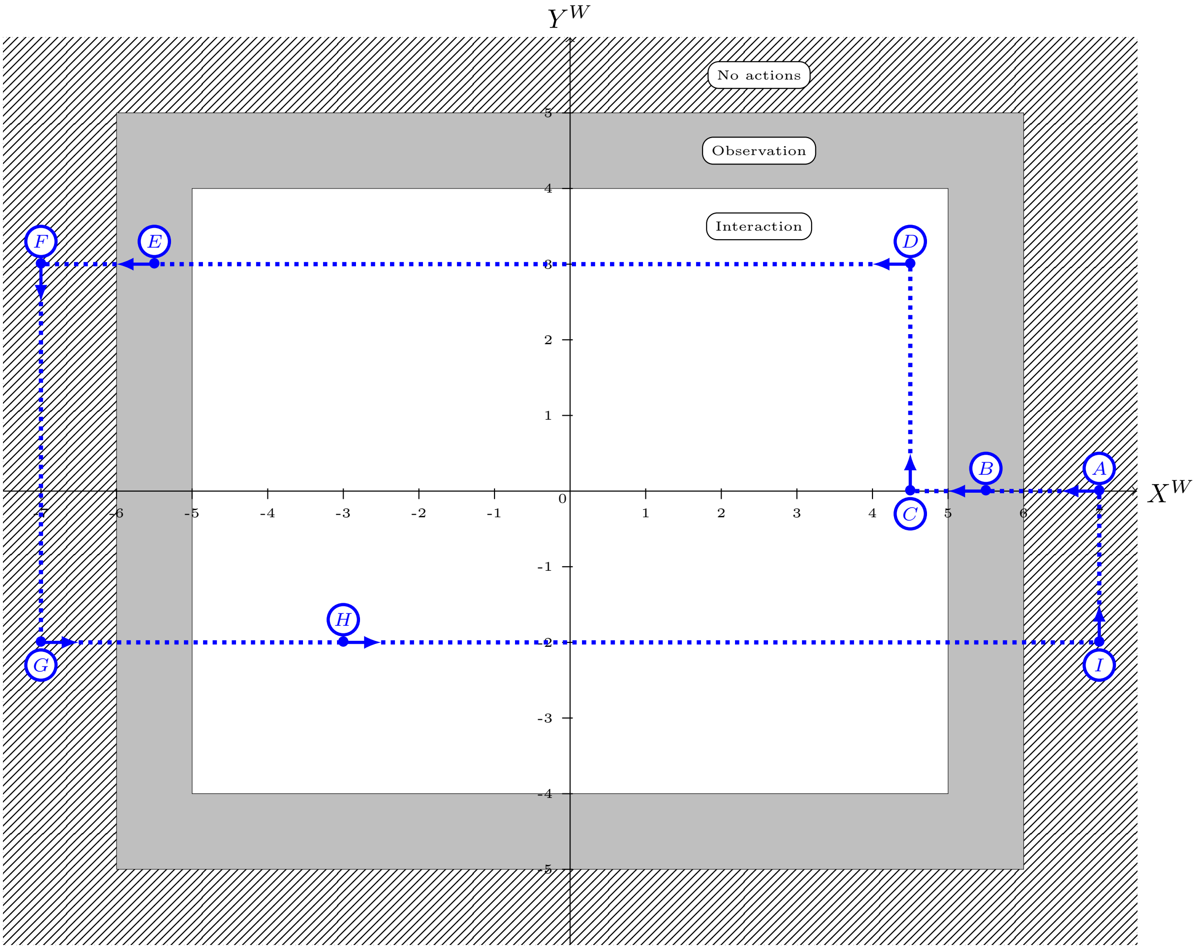

Figure 39 – Path P_1

Source – By author.

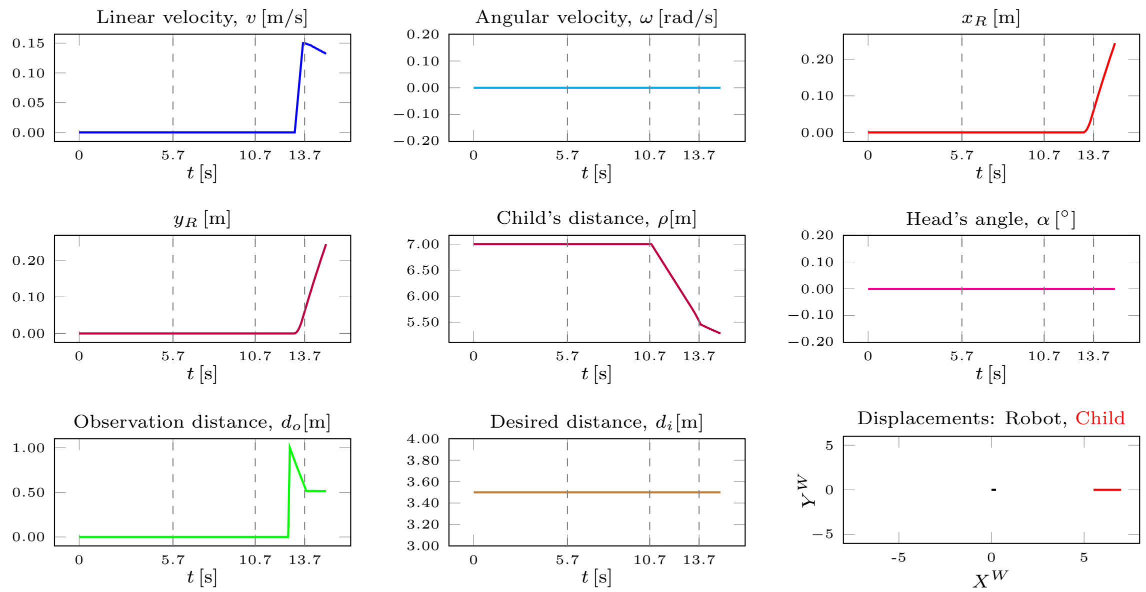

Figure 40 – Robot's data when the child goes from P_A to P_B

Source – By author.

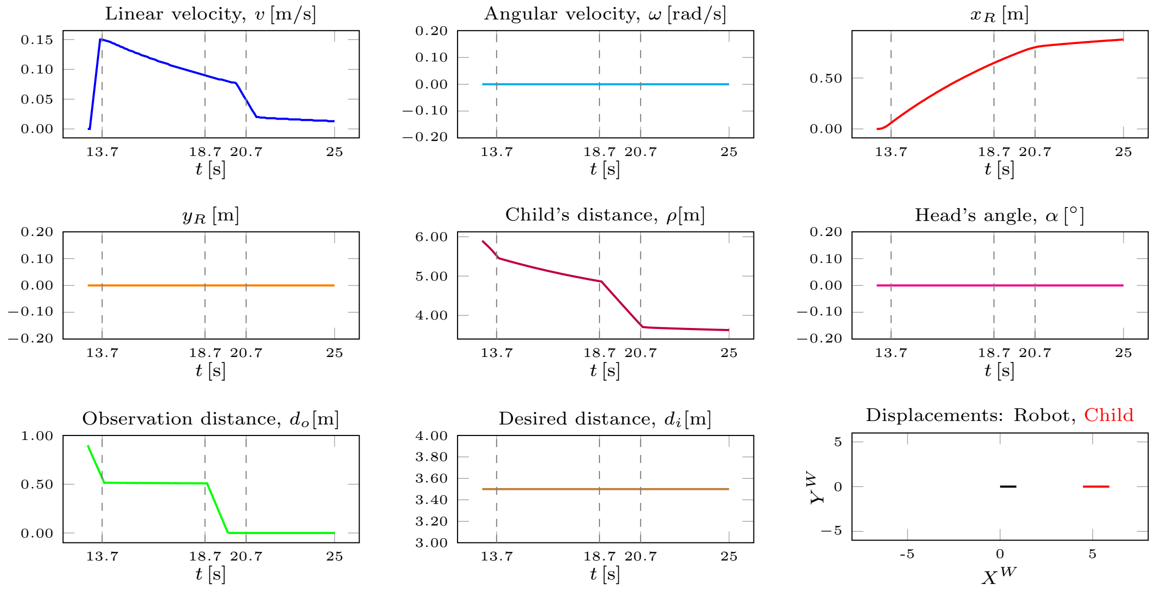

Figure 41 – Robot's data when the child goes from P_B to P_C

Source – By author.

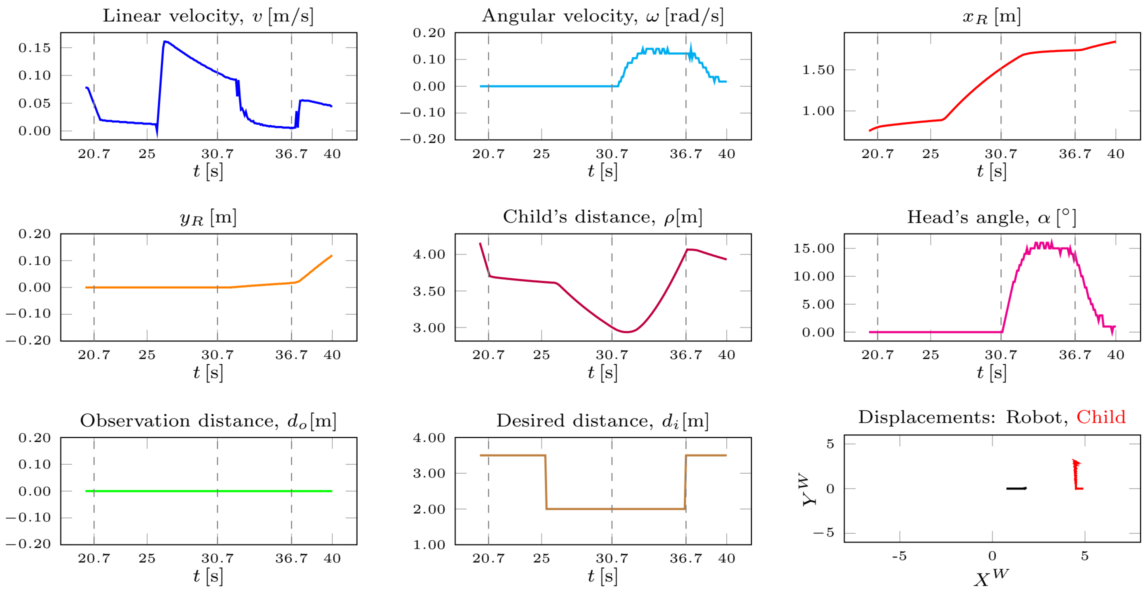

Figure 42 – Robot's data when the child goes from P_C to P_D

Source – By author.

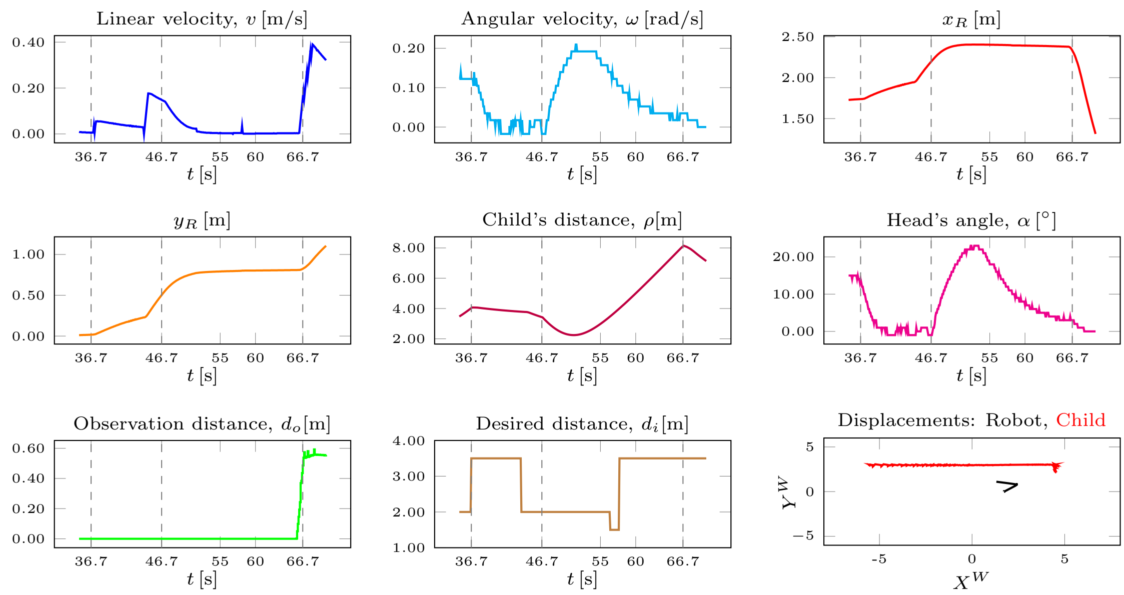

Figure 43 – Robot's data when the child goes from P_D to P_E

Source – By author.

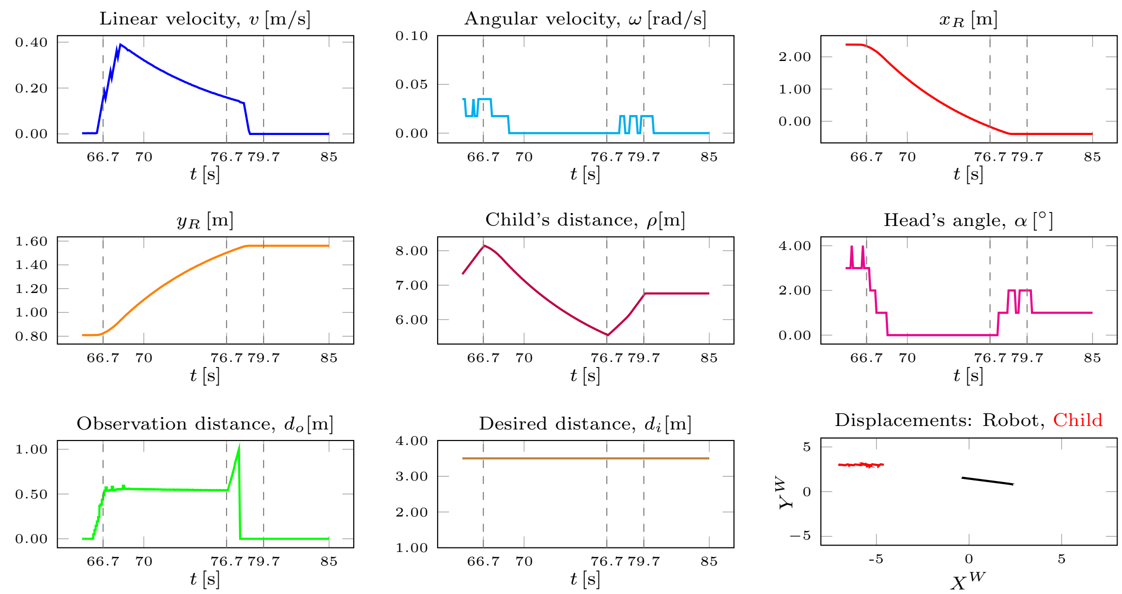

Figure 44 – Robot's data when the child goes from P_E to P_F

Source – By author.

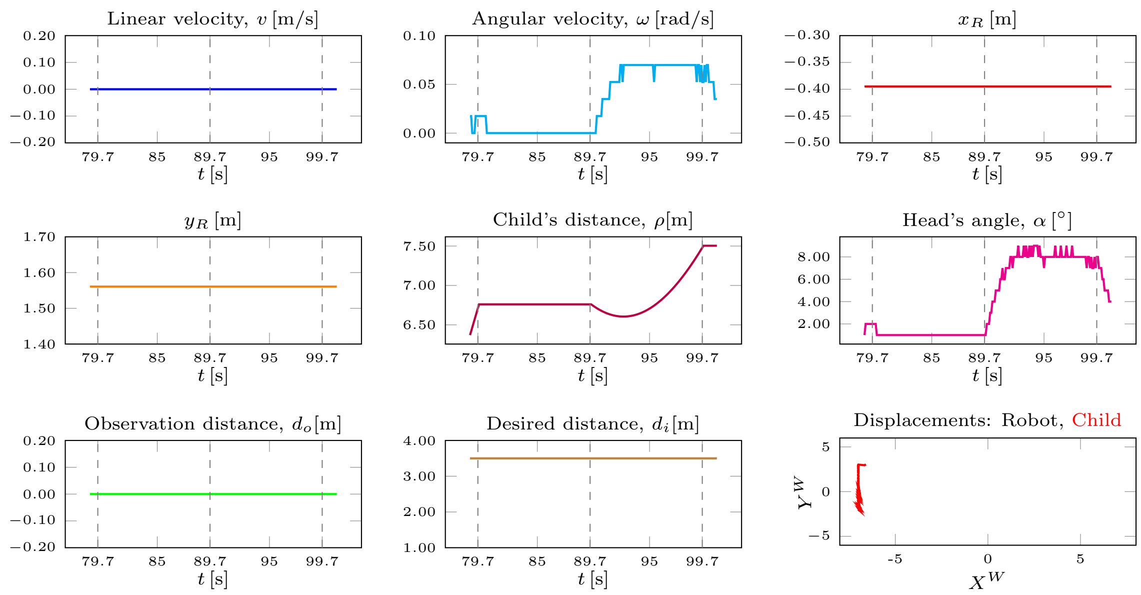

Figure 45 – Robot's data when the child goes from P_F to P_G

Source – By author.

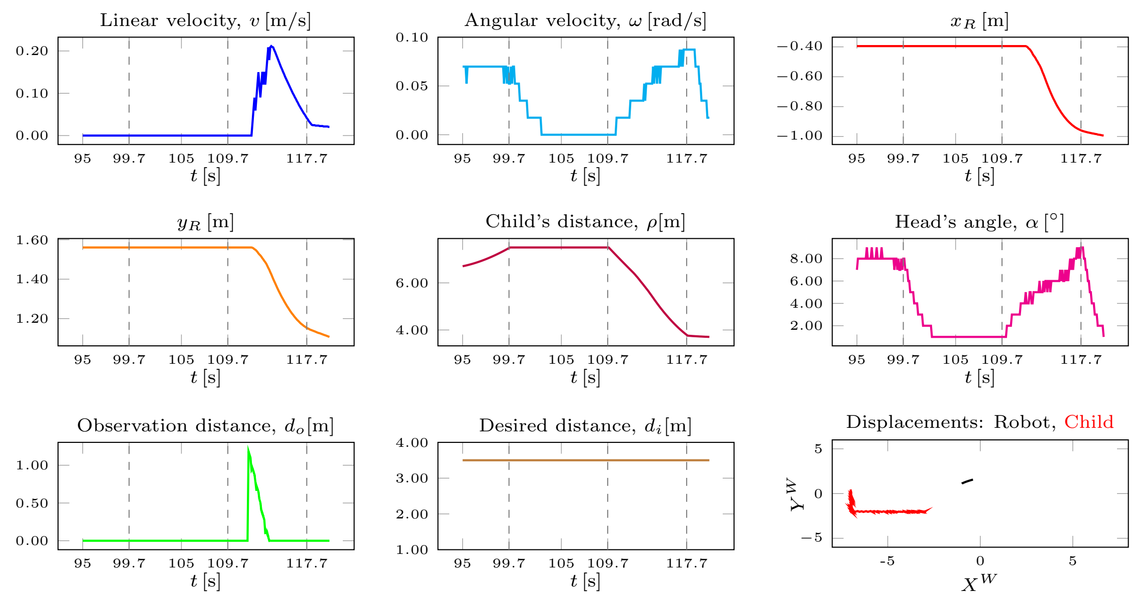

Figure 46 – Robot's data when the child goes from P_G to P_H

Source – By author.

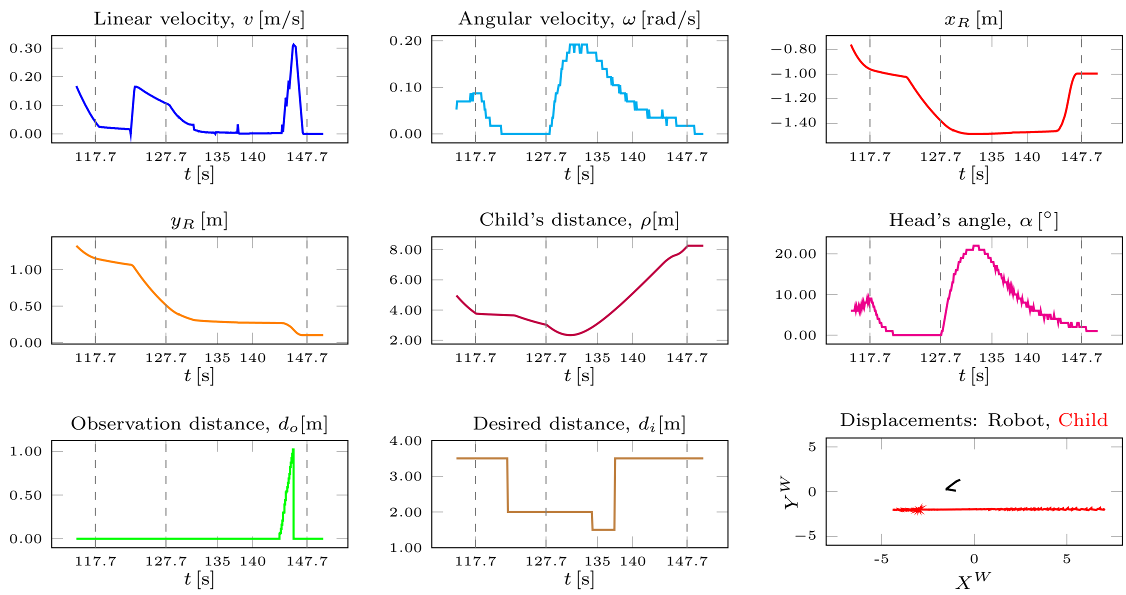

Figure 47 – Robot's data when the child goes from P_H to P_I

Source – By author.

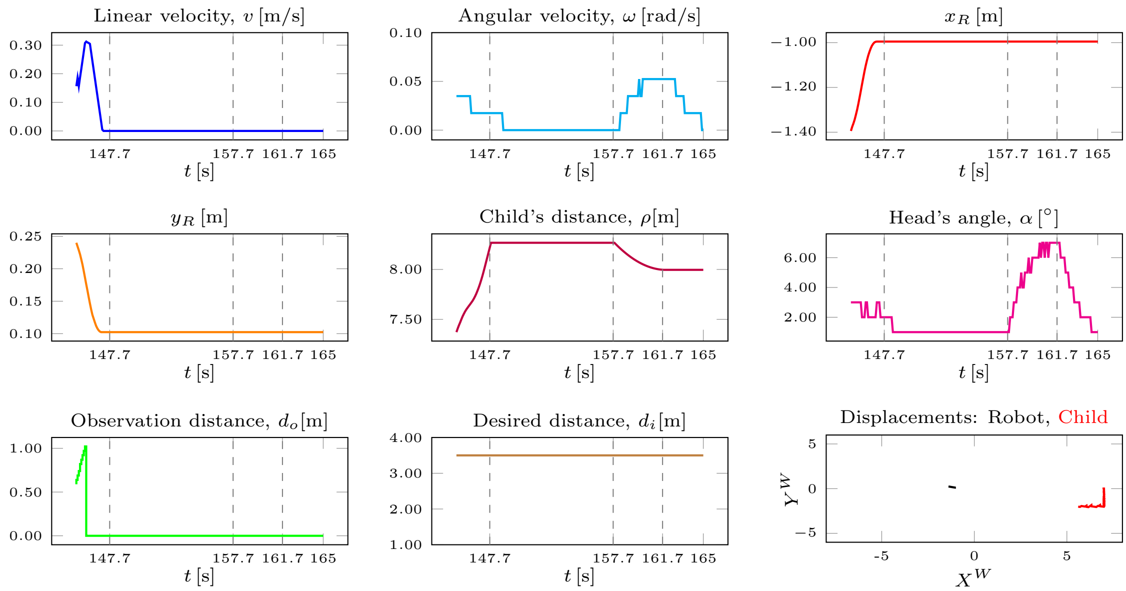

Figure 48 – Robot's data when the child goes from P_I to P_A

Source – By author.

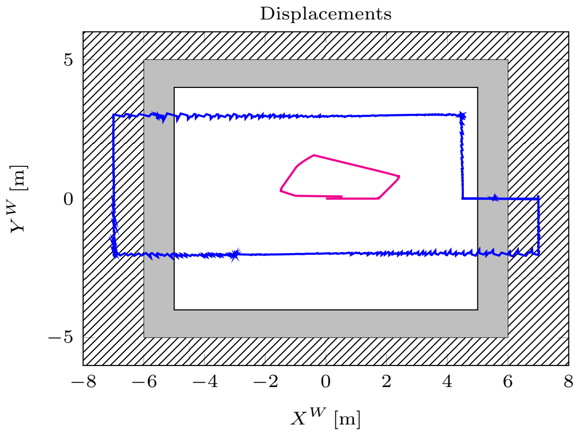

Figure 49 – Path P_1, Robot (in magenta) and Child's (in blue) displacements

Source – By author.

Figure 49 shows the robot's displacement while interacting with the child.

Figure 50 shows emotions calculated according to *State Machine* proposed. At $t = 27.4$ s the robot is near to the child and changes the proxemic zone to *social*, therefore the robot simulates a happiness of 50 %. On the other hand, at $t = 36.9$ s the child goes away and he/she increases the distance between himself/herself to the robot, and, therefore, the robot simulates a sadness of 100 %. The same behavior is observed at $t = 46.5$ s and $t = 58$ s, and at $t = 125$ s and $t = 137.8$ s.

4.1.4 Analysis of second *Path*

In this section the Path P_2 is analyzed (graphically represented in Figure 51). This path represents what occurs when the child stays most time in *observation area*.

Figures 52, 53, 54, 55, 56, 57, and 58 show the seven steps separately. In Figures 52 the child goes to interaction area and waits for robot's approach. This can be observed because child's distance from the robot changes from 7 m to 3.5 m. The approximation of the robot is visualized in Figure 53, where the linear velocity varies according to child's distance and desired distance.

Figures 54, 55, and 56 show the displacements of the child throw the *observation area*. In Figure 54 it is important to observe that at $t_7 = 88.8$ s the desired distance changes from 0.5 m to 3.5 m because the child is far away from the robot (which maintain its position). In Figure 55 is observed that during the time between $t_7 = 88.8$ s and $t_8 = 118.8$ s the child stills stopped and, therefore, the robot does not move. On the other hand, between $t_8 = 118.8$ s and $t_9 = 140.8$ s, the child goes from P_D to P_E and there is a little movement of the robot.

Figure 59 shows the robot's displacement while interacting with the child. Again, the robot respects the interaction area and never pushes the boundaries. Figure 60 shows

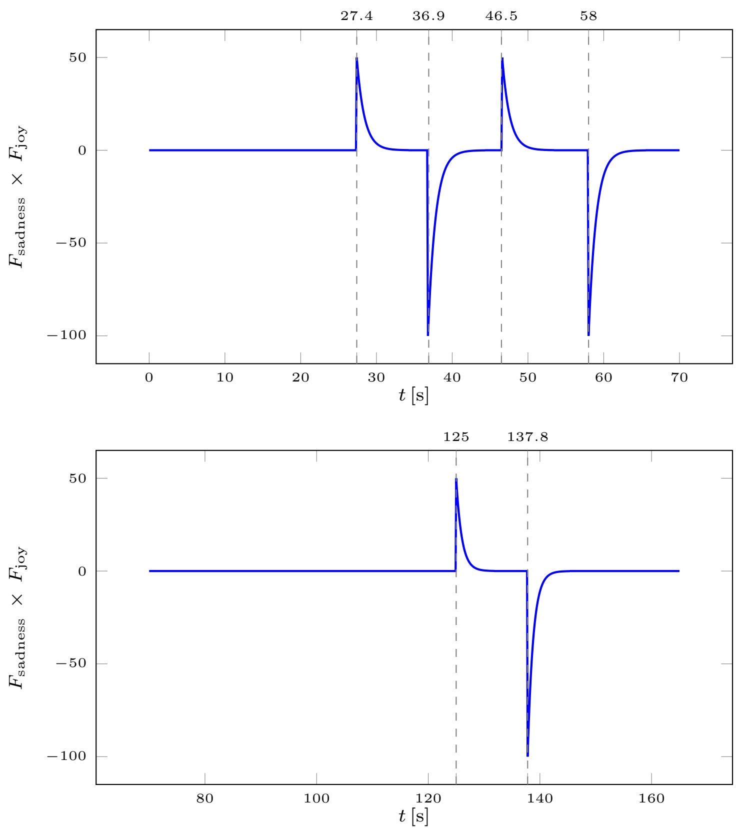

Figure 50 – Emotion calculated in path P_1

Source – By author.

the emotions calculated in simulation. In this case it is possible to observe that in addition to the emotions of joy and sadness, the emotion of fear is also calculated, due to the proximity of the robot to the edge. At $t_3 = 63.8$ s the robot is near to the limit of interaction area and starts to simulate a fear (which can be visualized in Figure 61). The presence of fear's emotion when there are joy or sadness causes the emotions of guilt and despair, respectively. This can be visualized in Figure 62.

4.2 RESULTS

According to simulations presented in Section 4.1, the proposal presented in this work allows the robot to maintain a proximity to the child always respecting her/him intentions.

Emotions were calculated as expected, respecting what was proposed in *Machine State*.

In the next chapter a conclusion of this work is made and some future features to be implement are proposed.

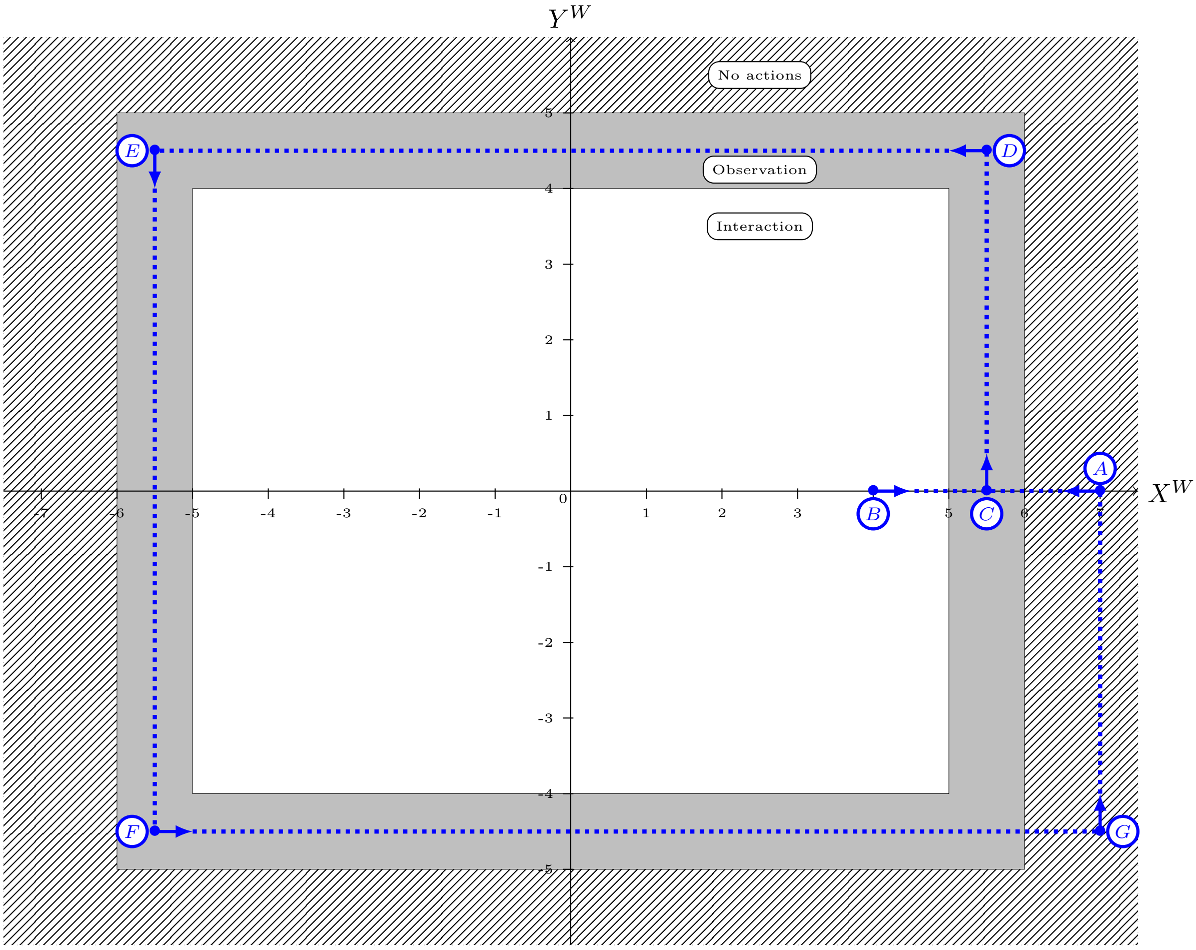

Figure 51 – Path P_2

Source – By author

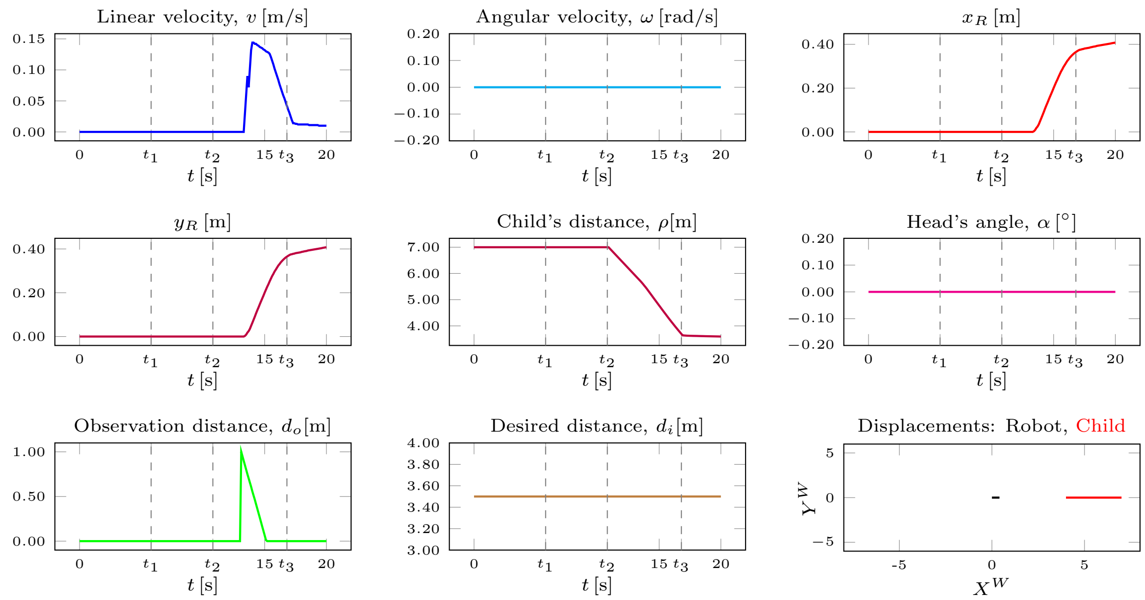

Figure 52 – Robot's data when the child goes from P_A to P_B

Source – By author.

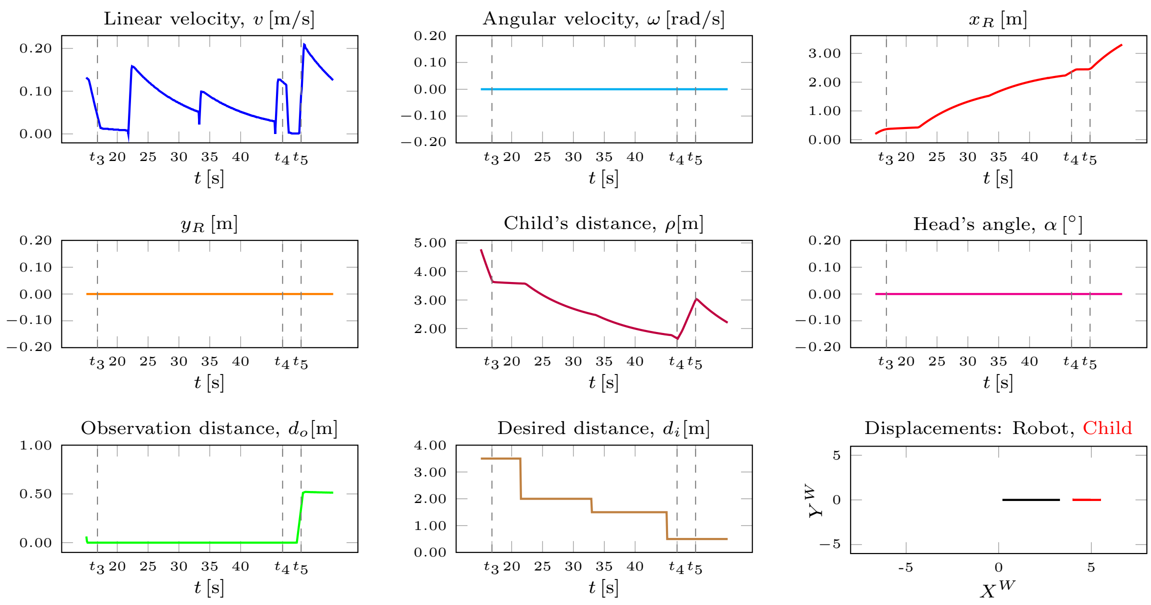

Figure 53 – Robot's data when the child goes from P_B to P_C

Source – By author.

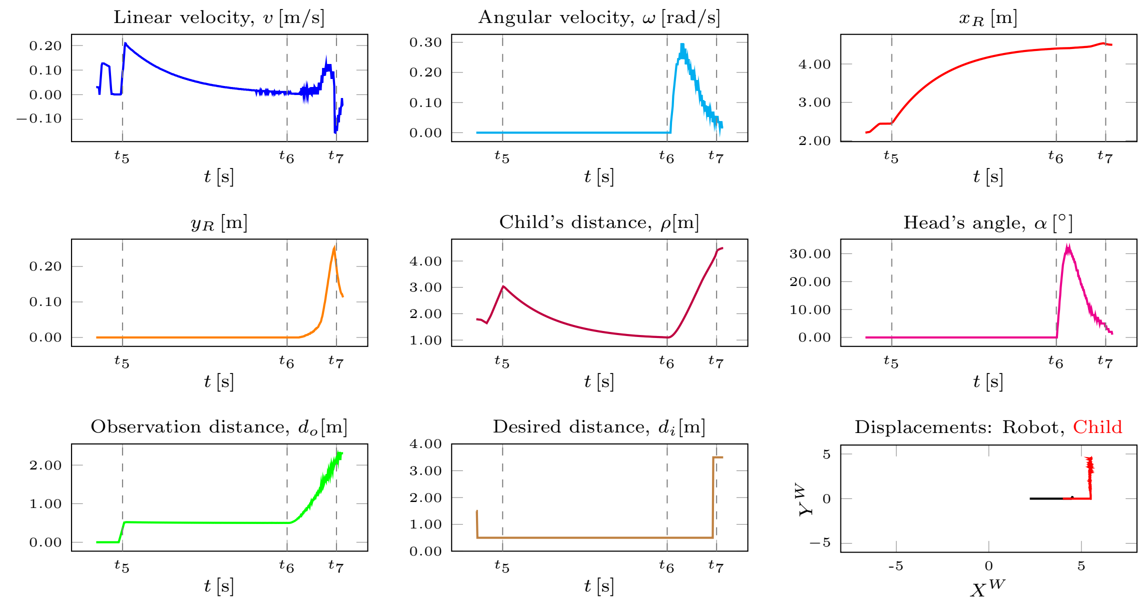

Figure 54 – Robot's data when the child goes from P_C to P_D

Source – By author.

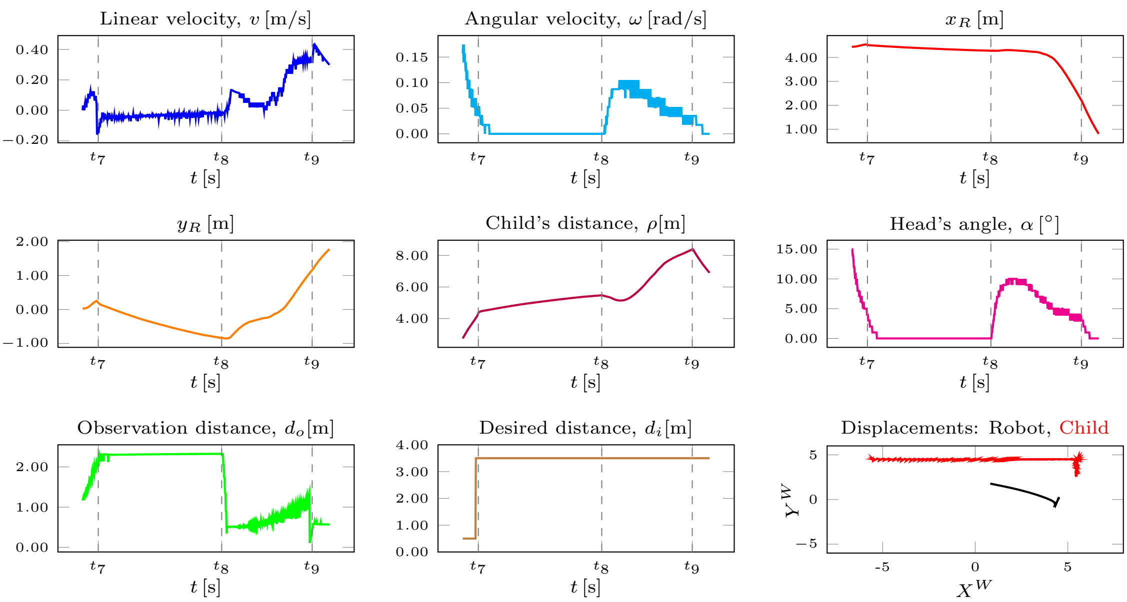

Figure 55 – Robot's data when the child goes from P_D to P_E

Source – By author.

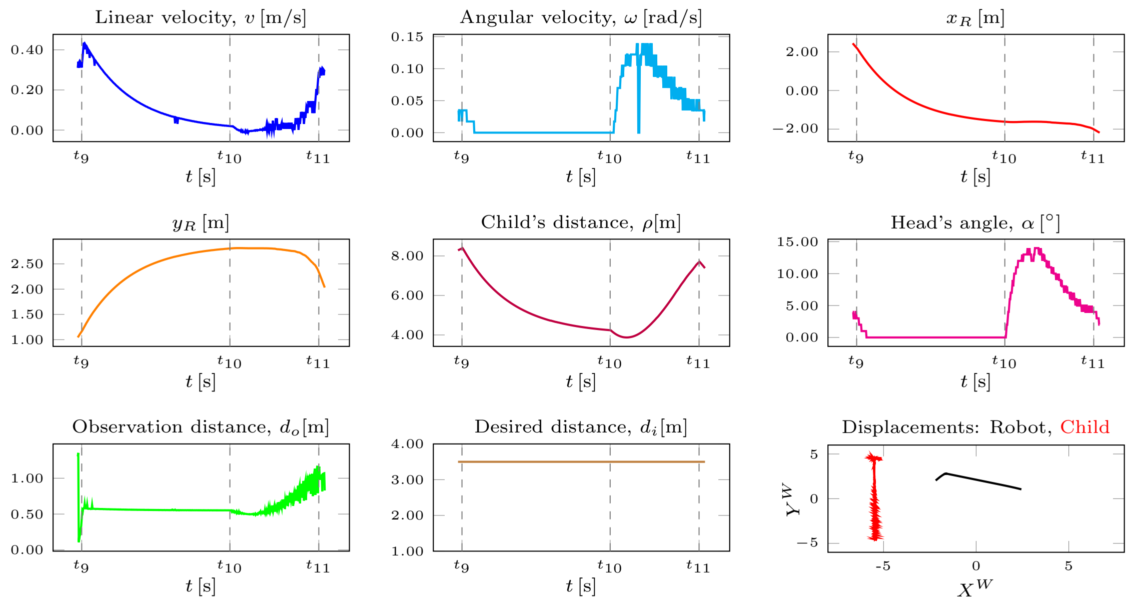

Figure 56 – Robot's data when the child goes from P_E to P_F

Source – By author.

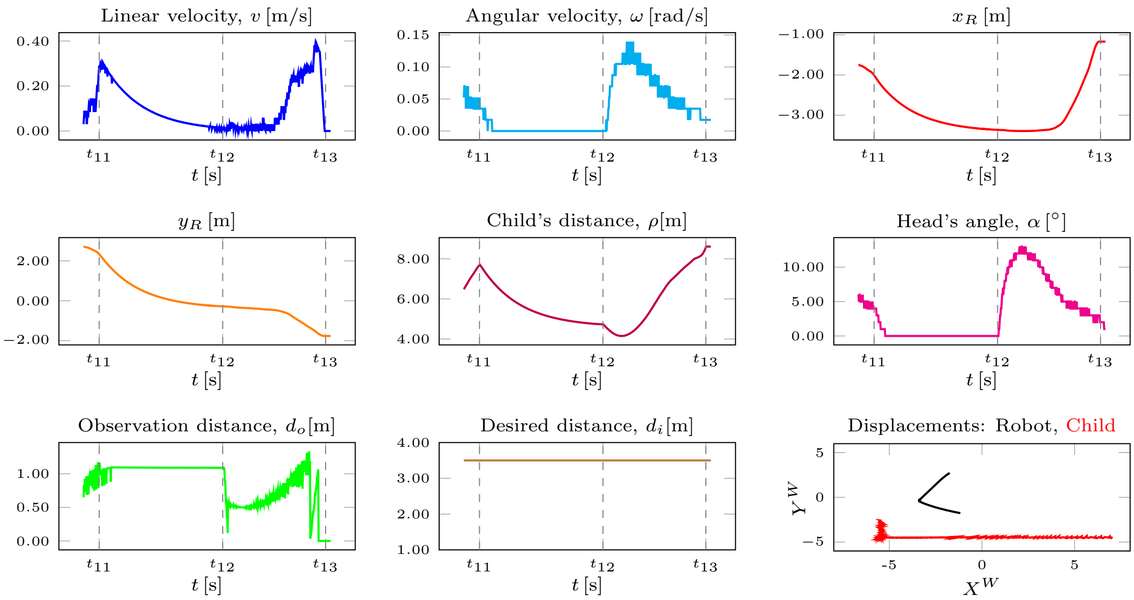

Figure 57 – Robot's data when the child goes from P_F to P_G

Source – By author.

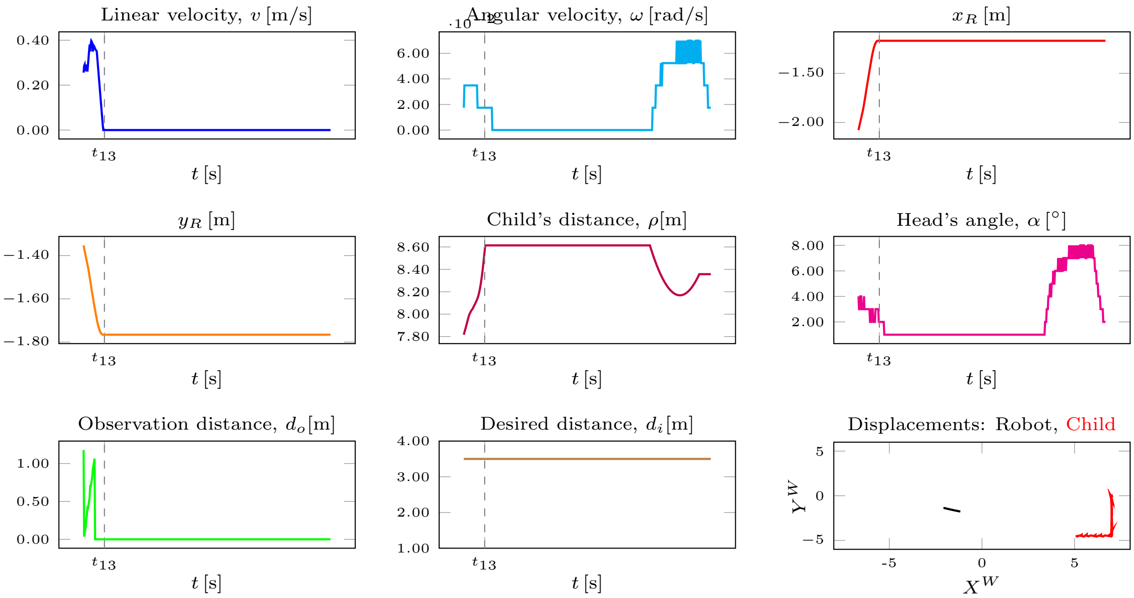

Figure 58 – Robot's data when the child goes from P_G to P_A

Source – By author.

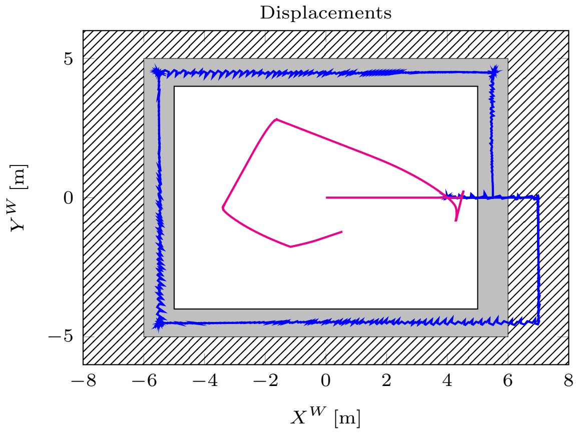

Figure 59 – Path P_2, Robot (in magenta) and Child's (in blue) displacements

Source – By author.

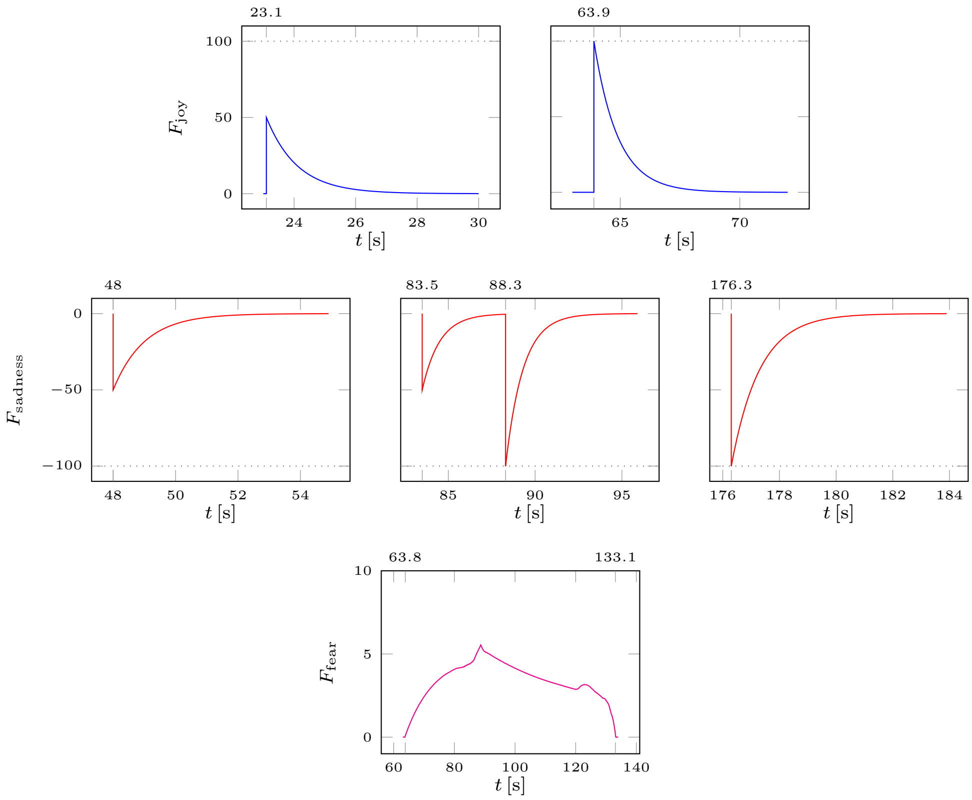

Figure 60 – Emotions calculated in the simulation

Source – By author.

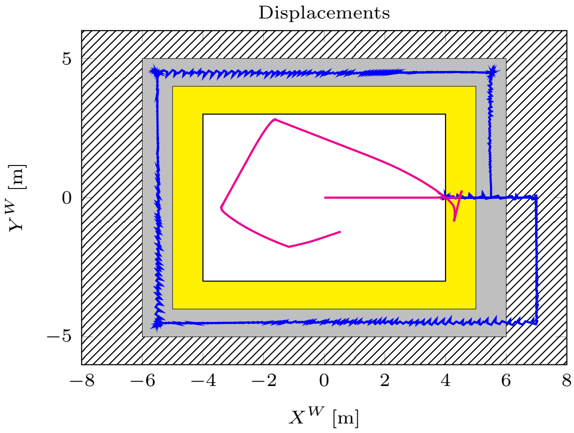

Figure 61 – Path P_2, Robot (in magenta) and Child's (in blue) displacements. In yellow is highlighted the area where the robot computes fear emotion because it is near to the edge of interaction area

Source – By author.

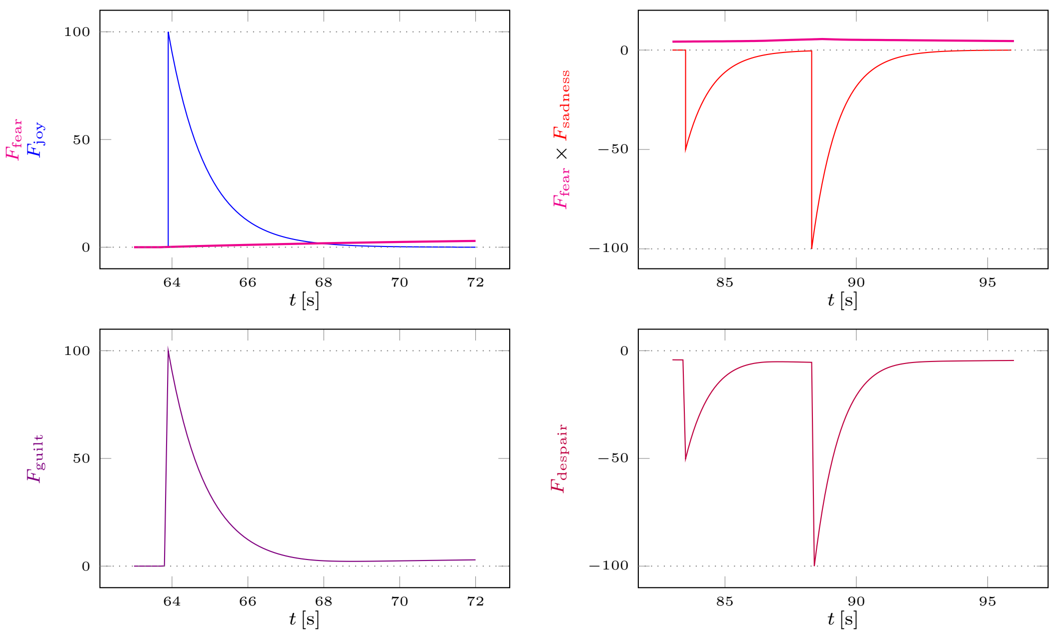

Figure 62 – Guilt and despair emotions calculated when there are fear emotion together with joy and sadness, respectively

Source – By author.

5 CONCLUSION

> [...] in all these things we are more than conquerors through him that loved us.
>
> Romans, 8, 37

This work presented concepts of *Workspace* and use of *proxemic zones* to propose a new control law to allow the robot to interact with children with ASD. Moreover, it was shown an internal representation of the emotional state and how this emotional state can be visualized as a robot's face.

The workspace divides the space in areas where the robot can follow the child or not, allowing a different interaction depending on the place the child is. A new control law was proposed in order to move the robot in the workspace, maintaining the proximity with the child, trying to look at his/her direction.

In this work, all system was implemented in ROS where nodes can be easily inserted or replaced, giving to the system a way to receive new behaviors, new modules. The code is available online[1].

Finally, an emotion representation was implemented in which the robot changes its emotion according to the child behavior, presented by himself/herself in the workspace area designed to have interaction or staying outside the interaction area, allowing or not robot approximation. Robot emotional state can be expressed in its face in order to give emotional feedback to the child, inducing his/her changes of behavior.

Considering the main objective of this Master's Dissertation, in spite of the system has been implemented only in simulated situations, it was possible to verify that the control law implemented allows the robot to maintain a friendly behavior near to the child. In addition, the concept of workspace makes the interaction space more safety, allowing the child to choose whether to stay close to or away from the robot.

5.1 FUTURE WORKS

There are a few points that need improvement: first, it is necessary to carry out tests with children with ASD (the *Coronavirus Pandemic* did not allow safely tests); in second place, it is necessary to observe how children respond to workspace and define limits; finally, it is important to analyze how children interact to faces created to simulate robot's emotions.

1 <https://drive.google.com/drive/folders/1n4g6GCdPncrs8Z7mm1a9KAGnfLgHxvw8?usp=sharing>

Some suggestions for future research are:

- Researching security for the Robot Operating System (DIEBER et al., 2017);
- Implementing emotions and facial expressions on `MARIA-T21`;
- Researching how the workspace impacts in children with ASD;
- Researching if `SAIBA` framework can be used in `MARIA-T21` (KOPP et al., 2006);
- Studying how basic emotions can be mixed in addition to the sum option used is this work;
- Studying how to use `pyplutchik` to represent emotional state graphically.

5.2 PUBLICATIONS

Two articles were published during the realization of this Master's Dissertation:

- Implementation of Dynamic Faces Based on Proxemics for Robot-ASD Children Interaction (PIERO et al., 2019);
- Use of Workspaces and Proxemics to Control Interaction Between Robot and Children with ASD (PIERO; CALDEIRA; BASTOS FILHO, 2020).

BIBLIOGRAPHY

ADĂSCĂLIŢEI, F.; DOROFTEI, I. Expressing emotions in social robotics-a schematic overview concerning the mechatronics aspects and design concepts. **IFAC Proceedings Volumes**, Elsevier, vol. 45, n. 6, p. 823–828, 2012.

BARNAUD, M.-L. et al. Proxemics models for human-aware navigation in robotics: Grounding interaction and personal space models in experimental data from psychology. In: **Proceedings of the 3rd IROS'2014 workshop "Assistance and Service Robotics in a Human Environment"**. [S.l.: s.n.], 2014.

BEREA, A. Introductory chapter: The role of communication as a fundamental process for life and society. In: BEREA, A. (Ed.). **A Complex Systems Perspective of Communication from Cells to Societies**. Rijeka: IntechOpen, 2019. cap. 1. Available from Internet: <https://doi.org/10.5772/intechopen.84721>.

BINOTTE, V. P. **Desenvolvimento de um Robô Socialmente Assistivo com Controle Baseado em Comportamento de Seleção de ação para Interação com Crianças com TEA**. Dissertation (Master's degree) — Federal University of Espirito Santo, Vitória, Brazil, 2018.

BOGUE, R. Robots in healthcare. **Industrial Robot: An International Journal**, Emerald Group Publishing Limited, 2011.

CABIBIHAN, J.-J. et al. Why robots? a survey on the roles and benefits of social robots in the therapy of children with autism. **International journal of social robotics**, Springer, vol. 5, n. 4, p. 593–618, 2013.

CARELLI, R. **Diseñño de Sistemas de Control no Lineal**. 2018. Retrieved Mar 20, 2018.

CASHMORE, M. et al. Rosplan: Planning in the robot operating system. In: **Proceedings of the International Conference on Automated Planning and Scheduling**. [S.l.: s.n.], 2015. vol. 25, n. 1.

CHEBOTAREVA, E. et al. Emotional social robot "emotico". In: . [S.l.: s.n.], 2019. p. 247–252.

CHEN, Y.; LEE, S. Y. M.; HUANG, C.-R. Automatic recognition of emotion based on a cognitively motivated emotion annotation system. **Journal of Cognitive Science**, vol. 12, n. 3, p. 279–298, 2011.

CLAVERO, J. G. et al. Defining adaptive proxemic zones for activity-aware navigation. In: SPRINGER. **Workshop of Physical Agents**. [S.l.], 2020. p. 3–17.

COCCIA, M. General properties of the evolution of research fields: a scientometric study of human microbiome, evolutionary robotics and astrobiology. **Scientometrics**, Springer, vol. 117, n. 2, p. 1265–1283, 2018.

COELHO, A. **The History of Robots in Healthcare [INFOGRAPHIC]**. 2014. Retrieved Aug 13, 2021. Available from Internet: <https://weatherbyhealthcare.com/blog/the-history-of-robots-in-healthcare-infographic>.

COPPIN, G.; SANDER, D. Contemporary theories and concepts in the psychology of emotions. In: ______. **Emotion-Oriented Systems**. [S.l.]: John Wiley & Sons, Ltd, 2013. cap. 1, p. 1–31. ISBN 9781118601938.

DALEY, S. et al. **Robotics. What is Robotics? What are Robots? Types & Uses of Robots.** 2021. Retrieved May 20, 2021. Available from Internet: <https://builtin.com/robotics>.

DATTALO, A. **ROS – Introduction**. 2018. Retrieved April 02, 2021. Available from Internet: <http://wiki.ros.org/ROS/Introduction>.

DIEBER, B. et al. Security for the robot operating system. **Robotics and Autonomous Systems**, Elsevier, vol. 98, p. 192–203, 2017.

DIEHL, J. J. et al. The clinical use of robots for individuals with autism spectrum disorders: A critical review. **Research in autism spectrum disorders**, Elsevier, vol. 6, n. 1, p. 249–262, 2012.

DUQUE, A. A. R. **From Robot-Assisted Intervention to New Generation of Autism Screening: An Engineering Implementation Beyond the Technical Approach**. Thesis (PhD) — Federal University of Espirito Santo, Vitória, 2019.

EKMAN, P.; FRIESEN, W. V. Constants across cultures in the face and emotion. **Journal of personality and social psychology**, American Psychological Association, vol. 17, n. 2, p. 124, 1971.

FEIDAKIS, M. et al. Affective assessment in distance learning: A semi-explicit approach. **International Journal of Technologies in Learning**, vol. 26, p. 19–34, 04 2019.

FEIL-SEIFER, D.; MATARIC, M. Defining socially assistive robotics. In: **9th International Conference on Rehabilitation Robotics, 2005. ICORR 2005.** [S.l.: s.n.], 2005. p. 465–468.

FRANCO, R. de L. L. D. **Análise Cinemática da Marcha de Crianças Diplégicas Nível I e II do GMFCS**. Dissertation (Master's degree) — Federal University of Minas Gerais, Belo Horizonte, Brazil, 2009.

GINÉS, J. et al. Social navigation in a cognitive architecture using dynamic proxemic zones. **Sensors**, Multidisciplinary Digital Publishing Institute, vol. 19, n. 23, p. 5189, 2019.

HALL, E. T. **The hidden dimension**. Doubleday, NY: Garden City, 1966. vol. 609.

Hanson Robotics. **Sophia**. 2021. Retrieved May 20, 2021. Available from Internet: <https://www.hansonrobotics.com/sophia/>.

HEDGES, R. **RosAria: Package Summary**. 2018. Retrieved May 08, 2021. Available from Internet: <http://wiki.ros.org/ROSARIA>.

HERRERA, D. et al. Cognitive social zones for improving the pedestrian collision avoidance with mobile robots. **Revista Politécnica**, Escuela Politécnica Nacional, vol. 42, n. 2, p. 7–14, 2019.

HERRERA, D. et al. Null-space based control for human following and social field avoidance. In: IEEE. **2017 XVII Workshop on Information Processing and Control (RPIC)**. [S.l.], 2017. p. 1–6.

HOCKSTEIN, N. G. et al. A history of robots: from science fiction to surgical robotics. **Journal of robotic surgery**, Springer, vol. 1, n. 2, p. 113–118, 2007.

HOLLINGER, G. A. et al. Design of a social mobile robot using emotion-based decision mechanisms. In: **2006 IEEE/RSJ International Conference on Intelligent Robots and Systems**. [S.l.: s.n.], 2006. p. 3093–3098.

ISMAIL, L. I. et al. Leveraging robotics research for children with autism: a review. **International Journal of Social Robotics**, Springer, vol. 11, n. 3, p. 389–410, 2019.

KAPUR, A. A history of robotic musical instruments. In: CITESEER. **ICMC**. [S.l.], 2005.

KERR, J.; NICKELS, K. Robot operating systems: Bridging the gap between human and robot. In: **Proceedings of the 2012 44th Southeastern Symposium on System Theory (SSST)**. [S.l.: s.n.], 2012. p. 99–104.

KOŁAKOWSKA, A. et al. Modeling emotions for affect-aware applications. In: WRYCZA, S. (Ed.). **Information Systems Development and Applications**. Sopot: Faculty of Management University of Gdańsk, 2015. cap. 4, p. 55–67.

KOPP, S. et al. Towards a common framework for multimodal generation: The behavior markup language. In: SPRINGER. **International workshop on intelligent virtual agents**. [S.l.], 2006. p. 205–217.

KOWALCZUK, Z.; CZUBENKO, M. Computational approaches to modeling artificial emotion – an overview of the proposed solutions. **Frontiers in Robotics and AI**, vol. 3, p. 21, 2016.

KROUPI, E.; YAZDANI, A.; EBRAHIMI, T. Eeg correlates of different emotional states elicited during watching music videos. In: SPRINGER. **International Conference on Affective Computing and Intelligent Interaction**. [S.l.], 2011. p. 457–466.

KUJAT, L. How have robotics impacted healthcare? **The Review: A Journal of Undergraduate Student Research**, vol. 12, n. 1, p. 6–8, 2010.

KUPPENS, P. et al. The relation between valence and arousal in subjective experience. **Psychological bulletin**, American Psychological Association, vol. 139, n. 4, p. 917, 2013.

LAZARUS, R. S.; LAZARUS, B. N. **Passion and reason: Making sense of our emotions**. [S.l.]: Oxford University Press, USA, 1994.

LEATHERS, D. G.; EAVES, M. H. **Successful Nonverbal Communication: Principles and Applications**. 4th. ed. New York, NY: Routledge, 2016.

LEE, T.-C. et al. Tracking control of unicycle-modeled mobile robots using a saturation feedback controller. **IEEE transactions on control systems technology**, IEEE, vol. 9, n. 2, p. 305–318, 2001.

LÖVHEIM, H. A new three-dimensional model for emotions and monoamine neurotransmitters. **Medical hypotheses**, Elsevier, vol. 78, n. 2, p. 341–348, 2012.

MALU, S. K.; MAJUMDAR, J. Kinematics, localization and control of differential drive mobile robot. **Global Journal of Research In Engineering**, 2014.

MARCUS, G. E. The psychology of emotion and politics. In: SEARS, D. O.; HUDDY, L.; JERVIS, R. (Ed.). **Oxford Handbook of Political Psychology**. [S.l.]: Oxford University Press, 2003. cap. 6, p. 182–221.

MATTHEWS, K. **The Growing Emergence of Robots in Healthcare: Key Opportunities & Benefits**. 2019. Retrieved Aug 13, 2021. Available from Internet: <https://hitconsultant.net/2019/12/05/the-growing-emergence-of-robots-in-healthcare-key-opportunities-benefits/#.YRbVp1tv9H4>.

MAVRIDIS, N. A review of verbal and non-verbal human–robot interactive communication. **Robotics and Autonomous Systems**, Elsevier, vol. 63, p. 22–35, 2015.

MEAD, R.; MATARIĆ, M. J. Autonomous human–robot proxemics: socially aware navigation based on interaction potential. **Autonomous Robots**, Springer, vol. 41, n. 5, p. 1189–1201, 2017.

MEHRABIAN, A.; RUSSELL, J. A. The basic emotional impact of environments. **Perceptual and motor skills**, SAGE Publications Sage CA: Los Angeles, CA, vol. 38, n. 1, p. 283–301, 1974.

MICHAUD, F.; CLAVET, A. Robotoy contest-designing mobile robotic toys for autistic children. **Proc. of the American Society for Engineering Education (ASEE'01)**, 2001.

MOREIRA, D. et al. Comparação da velocidade da marcha de crianças saudaveis em dois ambientes. **Lecturas: Educación física y deportes**, Tulio Guterman, n. 99, p. 11, 2006.

MUMM, J.; MUTLU, B. Human-robot proxemics: physical and psychological distancing in human-robot interaction. In: **Proceedings of the 6th international conference on Human-robot interaction**. [S.l.: s.n.], 2011. p. 331–338.

MYERS, D. G. **Psychology**. 10th. ed. [S.l.]: Worth Publishers, 2011.

NARVARTE, R. E. S. Comunicación y política en antonio pasquali. una lectura de comunicación y cultura de masas en el actual contexto latinoamericano. **Punto Cero**, UCB, vol. 19, n. 28, p. 45–52, 2014.

NOGUEIRA, P. **Piloto de ROV: profissão de grande potencial no mercado de petróleo**. 2017. Retrieved May 20, 2021. Available from Internet: <https://clickpetroleoegas.com.br/piloto-de-rov-profissao-de-grande-potencial-no-mercado-de-petroleo/>.

PAIVA, A.; LEITE, I.; RIBEIRO, T. Emotion modeling for social robots. **The Oxford handbook of affective computing**, p. 296–308, 2014.

PAIVA, A. et al. Towards more humane machines: Creating emotional social robots. **Towards more humane machines: creating emotional social robots**, Routledge, p. 125–139, 2018.

PANCERI, J. et al. Proposal of a new socially assistive robot with embedded serious games for therapy with children with autistic spectrum disorder and down syndrome. In: BASTOS FILHO, T. F.; CALDEIRA, E. M. de O.; FRIZERA NETO, A. (Ed.). **XXVII Brazilian Congress on Biomedical Engineering**. Vitória, Brazil: [s.n.], 2020. p. 1865–1870.

PARDÀS, M.; BONAFONTE, A. Facial animation parameters extraction and expression recognition using hidden markov models. **Signal Processing: Image Communication**, Elsevier, vol. 17, n. 9, p. 675–688, 2002.

PARRA, A. C. V. **Admittance Control of a Robotic Knee Orthosis based on Motion Intention through sEMG of Trunk Muscles**. Thesis (PhD) — Federal University of Espirito Santo, Vitória, 2017.

PENA, D.; TANAKA, F. Human perception of social robot's emotional states via facial and thermal expressions. **ACM Transactions on Human-Robot Interaction (THRI)**, ACM New York, NY, USA, vol. 9, n. 4, p. 1–19, 2020.

PHAN, D.-A.; SHINDO, H.; MATSUMOTO, Y. Multiple emotions detection in conversation transcripts. In: **Proceedings of the 30th Pacific Asia Conference on Language, Information and Computation: Oral Papers**. [S.l.: s.n.], 2016. p. 85–94.

PIERO, G. P. D.; CALDEIRA, E. M. de O.; BASTOS FILHO, T. F. Use of workspaces and proxemics to control interaction between robot and children with ASD. In: BASTOS FILHO, T. F.; CALDEIRA, E. M. de O.; FRIZERA NETO, A. (Ed.). **XXVII Brazilian Congress on Biomedical Engineering**. Vitória, Brazil: [s.n.], 2020. p. 1896–1901.

PIERO, G. P. D. et al. Implementation of dynamic faces based on proxemics for robot-ASD children interaction. In: GALOÁ. **Anais do 14º Simpósio Brasileiro de Automação Inteligente**. Ouro Preto, Brazil, 2019. vol. 1, p. 2675–2680. Available at https://proceedings.science/sbai-2019/papers/implementation-of-dynamic-faces-based-on-proxemics-for-robot-asd-children-interaction. Access on May, 16 2020.

PLUTCHIK, R. Emotion. **A psychoevolutionary synthesis**, Harper & Row, 1980.

PLUTCHIK, R. Integration, differentiation, and derivatives of emotion. In: RIEDL, R.; WIMMER, M. (Ed.). **Evolution and Cognition**. Klosterneuburg: Konrad Lorenz Institut für Evolutions- und Kognitionsforschung, 2001. p. 114–125.

PLUTCHIK, R. The nature of emotions: Human emotions have deep evolutionary roots, a fact that may explain their complexity and provide tools for clinical practice. **American scientist**, JSTOR, vol. 89, n. 4, p. 344–350, 2001.

POSNER, J.; RUSSELL, J. A.; PETERSON, B. S. The circumplex model of affect: An integrative approach to affective neuroscience, cognitive development, and psychopathology. **Development and psychopathology**, NIH Public Access, vol. 17, n. 3, p. 715, 2005.

PRASSLER, E. et al. A short history of cleaning robots. **Autonomous Robots**, Springer, vol. 9, n. 3, p. 211–226, 2000.

PREOŢIUC-PIETRO, D. et al. Modelling valence and arousal in facebook posts. In: **Proceedings of the 7th workshop on computational approaches to subjectivity, sentiment and social media analysis**. [S.l.: s.n.], 2016. p. 9–15.

QUIGLEY, M.; GERKEY, B.; SMART, W. D. **Programming Robots with ROS**. Sebastopol]: O'Reilly Media, 2015.

RATSAMEE, P. et al. Human–robot collision avoidance using a modified social force model with body pose and face orientation. **International Journal of Humanoid Robotics**, World Scientific, vol. 10, n. 01, p. 1350008, 2013.

RIOS-MARTINEZ, J.; SPALANZANI, A.; LAUGIER, C. From proxemics theory to socially-aware navigation: A survey. **International Journal of Social Robotics**, Springer, vol. 7, n. 2, p. 137–153, 2015.

ROBERT, J. **Hands-On Introduction to Robot Operating System (ROS)**. 2020. Retrieved April 02, 2021. Available from Internet: <https://trojrobert.github.io/hands-on-introdution-to-robot-operating-system(ros)/>.

ROBOTS and robotic devices — Vocabulary. Geneva, CH, 2012. vol. 2012.

RODRIGUES, P. S. L.; ASLA, S.; VELHO, L. Virtual emotion to expression: A comprehensive dynamic emotion model to facial expression generation using the mpeg-4 standard. In: ______. **Computer Animation**. Rio de Janeiro: Nova Science Publishers, 2009. cap. 6.

RÖSMANN, C. et al. Online trajectory prediction and planning for social robot navigation. In: IEEE. **2017 IEEE International Conference on Advanced Intelligent Mechatronics (AIM)**. [S.l.], 2017. p. 1255–1260.

RUBIO, F.; VALERO, F.; LLOPIS-ALBERT, C. A review of mobile robots: Concepts, methods, theoretical framework, and applications. **International Journal of Advanced Robotic Systems**, vol. 16, n. 2, p. 1729881419839596, 2019.

RUIJTEN, P. A.; CUIJPERS, R. H. Do not let the robot get too close: Investigating the shape and size of shared interaction space for two people in a conversation. **Information**, Multidisciplinary Digital Publishing Institute, vol. 11, n. 3, p. 147, 2020.

RUSSELL, J. A. A circumplex model of affect. **Journal of personality and social psychology**, American Psychological Association, vol. 39, n. 6, p. 1161, 1980.

SARTORATO, F.; PRZYBYLOWSKI, L.; SARKO, D. K. Improving therapeutic outcomes in autism spectrum disorders: Enhancing social communication and sensory processing through the use of interactive robots. **Journal of psychiatric research**, Elsevier, vol. 90, p. 1–11, 2017.

SATAKE, S. et al. Facilitating software development for mobile social robots by simulating interactions between a robot and pedestrians. In: **2019 14th ACM/IEEE International Conference on Human-Robot Interaction (HRI)**. [S.l.: s.n.], 2019. p. 626–627.

SCASSELLATI, B. How social robots will help us to diagnose, treat, and understand autism. In: **Robotics research**. [S.l.]: Springer, 2007. p. 552–563.

SCASSELLATI, B.; ADMONI, H.; MATARIĆ, M. Robots for use in autism research. **Annual review of biomedical engineering**, Annual Reviews, vol. 14, p. 275–294, 2012.

SCASSELLATI, B. et al. Improving social skills in children with ASD using a long-term, in-home social robot. **Science Robotics**, Science Robotics, vol. 3, n. 21, 2018.

SCASSELLATI, B.; VÁZQUEZ, M. The potential of socially assistive robots during infectious disease outbreaks. **Science Robotics**, Science Robotics, vol. 5, n. 44, 2020.

SCHERER, K. R. Measuring the meaning of emotion words: A domain-specific componential approach. Oxford University Press, 2013.

SEMERARO, A.; VILELLA, S.; RUFFO, G. Pyplutchik: visualising and comparing emotion-annotated corpora. **arXiv preprint arXiv:2105.04295**, 2021.

SILVA, G. V. M. **Controlo não linear**. 2006.

STONE, P. et al. **One Hundred Year Study on Artificial Intelligence**. Standford, CA, 2016.

TAHERI, A. et al. Social robots and teaching music to autistic children: Myth or reality? In: SPRINGER. **International conference on social robotics**. [S.l.], 2016. p. 541–550.

TAKAYAMA, L.; PANTOFARU, C. Influences on proxemic behaviors in human-robot interaction. In: IEEE. **2009 IEEE/RSJ International Conference on Intelligent Robots and Systems**. [S.l.], 2009. p. 5495–5502.

TAPUS, A.; MATARIC, M. J. Socially assistive robots: The link between personality, empathy, physiological signals, and task performance. In: **AAAI spring symposium: emotion, personality, and social behavior**. [S.l.: s.n.], 2008. p. 133–140.

TAPUS, A.; TAPUS, C.; MATARIC, M. J. The use of socially assistive robots in the design of intelligent cognitive therapies for people with dementia. In: **2009 IEEE International Conference on Rehabilitation Robotics**. [S.l.: s.n.], 2009. p. 924–929.

TARASENKO, S. Emotionally colorful reflexive games. **Computing Research Repository - CORR**, 12 2010.

TORBICO, D. M. **Identifying Emotions (Part 1)**. 2011. Retrieved April 02, 2021. Available from Internet: <https://acoarecovery.wordpress.com/2011/05/18/identifying-emotions-part-1>.

TSAROUCHI, P. et al. Robotized assembly process using dual arm robot. **Procedia CIrP**, Elsevier, vol. 23, p. 47–52, 2014.

VALADÃO, C. T. **Sistema de Supervisão e Controle para Interação Assistiva Humano-Robô**. Thesis (PhD) — Federal University of Espirito Santo, Vitória, 2016.

VERVISCH, T. et al. Oto – a diy platform for mobile social robots in education. In: LEPUSCHITZ, W. et al. (Ed.). **Robotics in Education**. Cham: Springer International Publishing, 2018. p. 257–262.

VITIELLO, A. et al. A neuro-fuzzy-bayesian approach for the adaptive control of robot proxemics behavior. In: IEEE. **2017 IEEE International Conference on Fuzzy Systems (FUZZ-IEEE)**. [S.l.], 2017. p. 1–6.

WALTERS, M. L. et al. An empirical framework for human-robot proxemics. **Procs of new frontiers in human-robot interaction**, 2009.

YATES, D. R.; VAESSEN, C.; ROUPRET, M. From leonardo to da vinci: the history of robot-assisted surgery in urology. **BJU international**, Blackwell Publishing Ltd Oxford, UK, vol. 108, n. 11, p. 1708–1713, 2011.

YEH, A. et al. Exploring proxemics for human-drone interaction. In: **Proceedings of the 5th international conference on human agent interaction**. [S.l.: s.n.], 2017. p. 81–88.

ZHANG, S. et al. Facial expression synthesis based on emotion dimensions for affective talking avatar. In: **Modeling Machine Emotions for Realizing Intelligence**. [S.l.]: Springer, 2010. p. 109–132.

ZHANG, Y. et al. Could social robots facilitate children with autism spectrum disorders in learning distrust and deception? **Computers in Human Behavior**, Elsevier, vol. 98, p. 140–149, 2019.

ZHOU, Y.; SHI, B. E. Photorealistic facial expression synthesis by the conditional difference adversarial autoencoder. In: IEEE. **2017 seventh international conference on affective computing and intelligent interaction (ACII)**. [S.l.], 2017. p. 370–376.

APPENDIX A – ROS MESSAGES

Listing A.1 – Custom Message Definition of `Position`

```
std_msgs/Header header
float64 x
float64 y
```

Listing A.2 – Custom Message Definition of `ChildDetection`

```
std_msgs/Header header
bool detected
float64 angle
float64 distance
general_functions/Position child_position
```

Listing A.3 – Custom Message Definition of `Workspace`

```
uint8 CHILD_AREA_EXTERNAL = 0
uint8 CHILD_AREA_OBSERVATION = 1
uint8 CHILD_AREA_INTERACTION = 2

Header   header
float64 child_observation_distance
uint8    child_area
float64 robot_bounds_proximity
```

Listing A.4 – Custom Message Definition of `OnChange`

```
Header header
uint8 PUBLIC = 0
uint8 SOCIAL_PUBLIC = 1
uint8 SOCIAL = 2
uint8 PERSONAL_SOCIAL = 3
uint8 PERSONAL = 4
uint8 last
uint8 current
```

Listing A.5 – Custom Message Definition of `DesiredDistance`

```
Header header
float64 desired_distance
```

Listing A.6 – Custom Message Definition of `EmotionDetection`

```
Header header
float64 x   # It is used for Joy-Sadness dimension
float64 y   # It is used for Trust-Disgust dimension
float64 z   # It is used for Fear-Anger dimension
float64 w   # It is used for Surprise-Anticipation
```